UC San Diego

UC San Diego Electronic Theses and Dissertations

Title

Ciliopathies : molecular and genetic basis for Ahi1 function in retinal degeneration

Permalink

https://escholarship.org/uc/item/4t10h3kg

Author

Louie, Carrie MC

Publication Date

2010

Peer reviewed|Thesis/dissertation

eScholarship.org Powered by the California Digital Library
University of California

UNIVERSITY OF CALIFORNIA, SAN DIEGO

Ciliopathies: Molecular and genetic basis for *Ahi1* function in retinal degeneration

A dissertation submitted in partial satisfaction of the
requirements for the degree Doctor of Philosophy

in

Biomedical Sciences

by

Carrie MC Louie

Committee in charge:

Professor Joseph G. Gleeson, Chair
Professor Lawrence S. Goldstein
Professor David S. Williams
Professor Anthony Wynshaw-Boris
Professor Kang Zhang
Professor Binhai Zheng

2010

The Dissertation of Carrie MC Louie is approved, and it is acceptable in quality and form for publication on microfilm and electronically:

_____

_____

_____

_____

_____

_____

Chair

University of California, San Diego

2010

DEDICATION

For my parents, who made so many

sacrifices to make this possible.

TABLE OF CONTENTS

LIST OF FIGURES

LIST OF TABLES

ACKNOWLEDGEMENTS

I would like to acknowledge Professor Joseph Gleeson for his support as the chair of my committee. I would also like to thank Professor David S. Williams, Lawrence Goldstein, Anthony Wynshaw-Boris, Binhai Zheng, and Kang Zhang for all of the guidance along the way.

Part of the introduction was published as: Louie, Carrie M; Gleeson, Joseph G. Genetic Basis of Joubert Syndrome and Related Disorders of Cerebellar Development. *Hum Mol Genet,* 14, Spec No. 2, R235-42, 2005. The dissertation author was the primary investigator and author of this paper.

Work in Chapters 2, 3, 4 was published as: Louie, Carrie M; Caridi, Gianluca; Lopes, Vanda S; Brancati, Francesco; Kispert, Andreas; Lancaster, Madeline A; Schlossman, Andrew M; Otto, Edgar A; Leitges, Michael; Hermann-Josef Gröne; Lopez, Irma; Gudiseva, Harini V; O'Toole, John F; Vallespin, Elena; Ayyagari, Radha; Ayuso, Carmen; Cremers, Frans PM; I den Hollander, Anneke; Koenekoop, Robert K; Dallapiccola, Bruno; Ghiggeri, Gian Marco; Hildebrandt, Friedhelm; Valente, Enza Maria; Williams, David S; Gleeson, Joseph G. *AHI1* is required for photoreceptor outer segment development and is a modifier for retinal degeneration in nephronophthisis. *Nature Genetics* vol. 42, p175-180 (2010); advance online publication, 17 Jan 2010 (doi:10.1038/ng.519). The dissertation author was the primary investigator and author of this paper.

VITA

2003 Bachelor of Science, Genetics, University of California, Davis
2003-2010 Research Assistant, University of California, San Diego

2005 Teaching Assistant, Department of Biology, University of California, San Diego

2010 Doctor of Philosophy, Biomedical Sciences, University of California, San Diego

PUBLICATIONS

Louie, Carrie M; Caridi, Gianluca; Lopes, Vanda S; Brancati, Francesco; Kispert, Andreas; Lancaster, Madeline A; Schlossman, Andrew M; Otto, Edgar A; Leitges, Michael; Hermann-Josef Gröne; Lopez, Irma; Gudiseva, Harini V; O'Toole, John F; Vallespin, Elena; Ayyagari, Radha; Ayuso, Carmen; Cremers, Frans PM; I den Hollander, Anneke; Koenekoop, Robert K; Dallapiccola, Bruno; Ghiggeri, Gian Marco; Hildebrandt, Friedhelm; Valente, Enza Maria; Williams, David S; Gleeson, Joseph G. *AHI1* is required for photoreceptor outer segment development and is a modifier for retinal degeneration in nephronophthisis. *Nature Genetics* vol. 42, p175-180 (2010); advance online publication, 17 Jan 2010 (doi:10.1038/ng.519)

Lancaster ML, Louie CM, Silhavy JL, Sintasath L, Decambre M, Nigam SK, Willert K, Gleeson JG. (2009) Impaired Wnt-beta-catenin signaling disrupts adult renal homeostasis and leads to cystic kidney ciliopathy. *Nat Med,* 15, 1046-54

Valente EM, Silhavy JL, Brancati F, Barrano G, Krishnaswami SR, Castori M, Lancaster MA, Boltshauser E, Boccone L, Al-Gazali L, Fazzi E, Signorini S, Louie CM, Bellacchio E; International Joubert Syndrome Related Disorders Study Group, Bertini E, Dallapiccola B, Gleeson JG. (2006) Mutations in Cep290, which encodes a centrosomal protein, cause pleiotropic forms of Joubert syndrome. *Nat Genet*, 36, 623-625

Louie, Carrie M; Gleeson, Joseph G. Genetic Basis of Joubert Syndrome and Related Disorders of Cerebellar Development. *Hum Mol Genet,* 14, Spec No. 2, R235-42, 2005

Dixon-Salazar TJ, Silhavy JL, Marsh SE, Louie CM, Scott LC, Gururaj A, Al-Gazali L, Al-Tawari AA, Kayserili H, Sztriha L, Gleeson JG. (2004). Mutations

in the *AHI1* Gene Encoding Jouberin, cause Joubert Syndrome with Cortical Polymicrogyria. *Am J Hum Genet*. 75, 979-87.

FIELDS OF STUDY

Major field: Biomedical Sciences

Studies in Genetics, Developmental Neuroscience, and Cell biology

ABSTRACT OF THE DISSERTATION

Ciliopathies: Molecular and genetic basis for role of *Ahi1* in retinal degeneration

by

Carrie MC Louie

Doctor of Philosophy in Biomedical Sciences

University of California, San Diego, 2010

Professor Joseph G. Gleeson, Chair

Ciliopathies comprise a highly heterogeneous group of genetic disorders attributed to dysfunction of the primary cilium. Joubert syndrome is a ciliopathy that primarily affects the central nervous system (CNS), and is specifically characterized by ataxia, hypotonia, and neonatal apnea associated

with cerebellar hypoplasia and malformation of the midbrain-hindbrain junction. Absence of *AHI1,* which encodes a cilium-localized protein, has been shown to cause a form of Joubert syndrome that is also highly penetrant for retinal degeneration[1,2], but the mechanisms underlying the pathogenesis of Joubert syndrome and related disorders are not well understood. To study the role of *Ahi1* in a more tractable model, I have targeted the *Ahi1* gene in the mouse to generate germline and conditional null alleles, and used tissue culture, mouse genetic analysis, histopathology and immunochemical techniques to study these mouse mutants. In contrast to human patients with the disease, brains from *Ahi1-/-* mice were nominally affected. Despite this, analysis of retina from *Ahi1-/-* mice revealed a phenotype consistent with the retinal involvement frequently observed in patients with deleterious *AHI1* mutations. Specifically, *Ahi1* knockout mice failed to form outer segments (OS), and showed abnormal distribution of opsin throughout photoreceptors. This was followed by rapid degeneration of the outer nuclear layer through apoptotic mechanisms attributed to the ectopic accumulation of opsin. Through analysis of double mutant mouse lines, I also found that the phenotype displayed dosage-sensitive genetic interactions with *Nphp1,* another ciliopathy gene. Although not a primary cause of retinal blindness in humans, I found that an allele of *AHI1* modifies the relative risk of retinal degeneration greater than 7 fold within a cohort of nephronopthisis patients. These data support context-specific roles for *AHI1* as a contributor to

retinopathy and may explain a proportion of the variability of retinal phenotypes observed in nephronophthisis.

CHAPTER 1: INTRODUCTION

ABSTRACT

Over three decades have passed since Marie Joubert described the original proband for Joubert syndrome, a rare neurological disorder featuring absence of the cerebellar vermis (i.e. midline). Efforts at deciphering the molecular basis for this disease have been complicated by the clinical and genetic heterogeneity as well as extensive phenotypic overlap with other syndromes. However, progress has been made in recent years with the mapping and identification of mutations in numerous genes, including *AHI1* and *NPHP1*. These genes encode proteins with some shared functional domains, but their role in brain development is unclear. Clues may come from studies of related syndromes, including Bardet–Biedl syndrome and nephronophthisis, for which all of the encoded proteins localize to primary cilia. The data suggest a tantalizing connection between intraflagellar transport in cilia and neurological disease.

CILIOPATHY DEFINED

A ciliopathy can be broadly defined as a genetic disorder of the cilium and/or basal body[3]. Cilia are microtubule-based structures usually projecting from the apical surface of cells and consisting of nine doublets of microtubules ensheathed in a plasma membrane. Motile cilia have a central pair of microtubule doublets as well as radial spokes and dynein arms which cooperate to generate

a beating motion. Primary, or nonmotile cilia are devoid of these features[4]. Classically, cilia and flagella were known to function in generating fluid flow or locomotion, but a plethora of recent evidence supports many specialized functions for these organelles. Furthermore, cilia have been identified on virtually every vertebrate cell type studied. Differences in their function and/or regulation may explain the diversity of phenotypes in ciliopathic disease.

Intraflagellar transport (IFT)

IFT is a highly conserved process needed for the formation and maintenance of cilia and flagella. This movement along the cilium was first observed in *Chlamydomonas* flagella[5] and was found to involve two major complexes of proteins associated with molecular motors. Anterograde transport into the cilium is mediated by a kinesin 2 family heterotrimeric complex of proteins[6], and retrograde transport from the tip of the cilium is mediated by a cytoplasmic dynein, IFT-dynein[7,8]. These complexes, termed IFT particles, were found to contain a core of highly conserved proteins needed for cilia assembly in other organisms[7]. Besides the core components of IFT, a large number of proteins have been localized to the cilium based on studies on individual proteins as well as proteomic and comparative genomic analysis[9-12].

IFT has generated particular interest in light of the recent implication of IFT proteins in the hedgehog signaling pathway, critical for many developmental processes. In an ENU mutagenesis screen for phenotypes resembling defective hedgehog signaling in mouse, Huangfu et al.[13] demonstrated the requirement for

IFT proteins (IFT88, IFT172) in normal hedgehog signaling downstream of its receptor Patched. Liu et al.[14]found that they act upstream of the proteolytic processing of Gli proteins, the transcriptional effectors of the Hh pathway. Several studies following this further refined the pathway, localizing many components of the Shh pathway to the cilium, including Smo, Ptc1, Gli2, Gli3, and finding that IFT is needed to process Gli3 from the activator to the repressor form[15-17].

CLINICAL FEATURES

Joubert syndrome (JS) is an autosomal recessive neurodevelopmental disorder, which is characterized by the molar tooth malformation (MTM), a complex brainstem malformation that reflects aplasia or marked hypoplasia of the cerebellar vermis, thickened and elongated superior cerebellar peduncles and a deepened interpeduncular fossa that is apparent on axial MRI at the midbrain–hindbrain junction (Figure 1.1)[18]. Clinically, classic JS is associated with neonatal hypotonia (loss of muscle tone), ataxia, developmental delay, mental retardation, and often neonatal apnea/hyperpnea (irregular breathing) and/or ocular motor apraxia (difficulties in initiating rapid horizontal eye movements—saccades)[19-21]. Autistic features have also been reported as a relatively common component of JS[22,23]. None of these features alone is diagnostic of JS, however, and in more recent years, it has become obvious that JS is a part of a spectrum of disorders involving vermis hypoplasia and the MTM. Some of these include COACH (OMIM 216360), referring to characteristic hallmarks of cerebellar vermis

hypoplasia, oligophrenia (mental impairment), congenital ataxia, ocular coloboma and hepatic fibrosis [24-26]; and Váradi Papp or orofaciodigital VI syndrome (OMIM 277170), defined by midline facial or hand abnormalities[24,27]. Varying degrees of extra-CNS involvement have further complicated diagnosis, including ocular colobomas, postaxial polydactyly, liver fibrosis, cystic dysplastic kidneys, retinal degeneration and/or nephronophthisis (NPHP)[24,28-34]. These features significantly overlap with other disorders with cerebello-oculo-renal involvement, most notably NPHP; the significance of this relationship is strengthened by the identification of deletions of *NPHP1*, a gene commonly mutated in NPHP in a subset of JS patients[35,36].

OVERVIEW OF CEREBELLAR DEVELOPMENT

Understanding of cerebellar development provides some insights into the pathogenesis of JS. The cerebellum arises from both the mesencephalic and rhombencephalic vesicles of the neural tube and develops over a relatively long period of time between early embryogenesis and late childhood[37,38]. Development of the cerebellum can be described in four basic stages. In the first stage, characterization of cerebellar territory occurs at the midbrain–hindbrain boundary. Transplantation studies in chicken and mouse have found that the isthmus organizer (IsO), a region corresponding to the midbrain– hindbrain boundary expression, is crucial for specifying midbrain and cerebellar structures[39]. At the isthmus, restricted expression of secreted factors, such as fibroblast growth factor 8, fgf8[40,41] and Wnt1, the mammalian homolog of

Drosophila wingless gene[42], as well as homeobox proteins En1 and En2 [43,44] and paired box genes Pax2 and Pax5[45,46] are required for early specification of midbrain and hindbrain structures[47]. In the second stage, two compartments for cell proliferation are formed. Purkinje cells and cells of the deep cerebellar nuclei are generated in the roof of the fourth ventricle[48,49], and granule cell precursors, as well as cells of the precerebellar nuclei are formed in the rhombic lip[50]. Purkinje cells are known to secrete Sonic hedgehog which regulates proliferation of granule cells[51,52]. By this time point, granule neuron precursors express a number of markers, *Math1*, *nestin*, *zipro1/RU49* and *Zic* genes 1, 2[53-56]. Purkinje cells migrate radially to their final positions, whereas granule neurons migrate over the surface of the developing cerebellum, forming the external granule layer (EGL) (Figure 1.2A and B). In the third stage, cells of the EGL migrate inward along the processes of Bergman glia to their final position in the internal granular layer (IGL)[57]. Finally, cerebellar circuitry is established and further differentiation occurs. The lower portion of the rhombic lip also gives rise to cells of the precerebellar nuclei such as the inferior olivary nuclei, which migrate to positions in the brainstem[58].

NEUROPATHOLOGY

There have been few detailed studies of neuropathology in JS patients, but various abnormalities have been identified as common to JS, affecting a number of systems in the midbrain and hindbrain. The most striking is the absence of the cerebellar vermis, thought to be important for control of balance,

regulation of muscle tone and saccadic (rapid) eye movements, although it should be noted that many lesions of the cerebellum could have this effect. The dentate nuclei, the major source of cerebellar output to the cerebral cortex, are fragmented into islands. Malformation of various pontine and medullary structures, including the basis pontis, reticular formation, inferior olivary, dorsal column and solitary tract nuclei, have been reported, which may explain the respiratory defects in JS[19,59]. Heterotopias of Purkinje-like neurons have been described in some patients, suggesting a migration defect[19]. Defects of proliferation are also likely, considering the absence of the vermis as well as the report of diminished density of granule neurons[19]. An interesting abnormality is the absence of decussation both of the superior cerebellar peduncles and of the corticospinal tracts at the medullary pyramids, which suggests that JS patients may have a defect of axon guidance. The pyramidal decussation is the site where the majority of corticospinal tracts cross at the midline[60]. The tract arises from the layer V pyramidal motor neurons of the cortex and extends through to the spinal cord. Fibers that reach and crossover at the cervicomedullary junction (CMJ) in the brainstem are referred to as the lateral CST, which convey motor signals from the brain. In contrast, the spinocortical somatosensory tract (SCT) is an ascending pathway that relays sensory signals back to the brain[61]. Defects in crossing over suggest that JS patients may display altered brain wiring. Indeed, a study on fMRI patterns reveals more bilateral activation in a JS patient versus a control, which is consistent with a defect of neural connectivity[62]. In total, the

pathology of JS seems to reflect abnormalities in a variety of events, suggesting that the genes involved are acting early in brain development.

RELATED DISORDERS

The range of the JS phenotype often involves systems outside the CNS and significantly overlaps with other disorders, for some of which, genes have been identified. The similarities in phenotype suggest that shared or similar pathways are affected in these disorders. Studying the functions of these genes may contribute to our understanding of JS. Interestingly, most of these genes have been shown to function in the cilia and/or intraflagellar transport (IFT).

Nephronophthisis (NPHP)

NPHP is a kidney disorder that represents the most common heritable cause of end-stage renal disease in children and is characterized by tubular atrophy, interstitial fibrosis and development of renal cysts. NPHP is a frequent involvement in JS cases and also exhibits substantial genetic overlap. There are 10 genes known to cause several forms of NPHP[63-65], namely, *NPHP1*[66], *INVS*[67], *NPHP3*[68], *NPHP4*[69], *IQCB1*[70], *CEP290*[71,72], *GLIS2*[73], *RPGRIP1L*[74], *NEK8*[75], and *TMEM67*[65], of which four are in common with JS. Juvenile NPHP is most often caused by mutations in *NPHP1*, encoding nephrocystin[66]. The most common mutation is a homozygous deletion that spans three contiguous genes presumably owing to the presence of flanking inverted repeat sequences. A subset of JS patients selected on the basis of kidney and/or retinal involvement

were recently screened for mutations and the common NPHP1 deletion was identified as a rare cause of JS[35,36]. Conversely, cerebellar malformations have been identified in patients diagnosed with NPHP[76]. All of the NPHP genes have been localized to primary cilia of renal epithelial cells and largely at the basal bodies, 8ransduc centrioles that form the base of cilia[67-70,77]. *NPHP2*, encoding inversin, a known cilia-related protein mutated in infantile NPHP, was the first direct evidence of involvement of cilia function in NPHP[67]. In *invs* mutant mice, the phenotype includes large kidney cysts and abnormalities in left–right patterning, situs inversus, in which organs have reverse orientation[78]. This unusual phenotype is due to abnormalities of leftward nodal flow, generated by monocilia that line the ventral surface of the embryonic node[79,80]. Furthermore, *nephrocystin-1* and *-4* homologs in Caenorhabditis elegans, which do not have a renal system, have been localized exclusively to ciliated sensory neurons, suggesting that they have conserved roles in ciliary function[81]. Nephrocystins have also been identified in other cellular compartments that implicate them in other functions including cell matrix signaling and cell division. *NPHP1* and *NPHP4* have been demonstrated to interact and form complexes with focal adhesion and cell–cell adherens junction proteins and localize to the subcortical region close to cell–cell junctions in polarized renal epithelial cells, as well as to the centrosome in confluent cells[77]. Inversin was shown to interact with Ncadherin and catenins at the plasma membrane and a shorter isoform has been detected in the nucleus where it interacts with *b*-catenin in a proximal tubule kidney cell line[82]. It has also been localized to the centrosome in early prophase

and to mitotic spindle poles in metaphase, where it interacts with the anaphase promoting complex 2, Apc2[83]. Intriguingly, a recent study suggests that inversin may be involved in the Wnt pathway by switching off the canonical pathway at the level of Dvl1[84]. The phenotypes of JS and NPHP also overlap with that of several other disorders for which the MTM can be identified as a component. Seniör –Loken syndrome (OMIM 266900) consists of the MTM, and NPHP with retinal aplasia like Leber congenital amaurosis, and has been associated with mutations in *NPHP1* and *NPHP4*[85]. The recently identified nephrocystin-5 or *ICQB1*, which shares functional domains with inversin, appears to be the most common cause of Seniör –Loken, further supporting the connection between the MTM and the NPHP genes[70]. Also closely related is Dekaban–Arima syndrome (OMIM 243910), associated with vermis aplasia, retinopathy and cystic dysplastic kidneys[86]. This syndrome has been traditionally distinguished from Seniör–Loken by its less severe kidney disease, but more recent analysis suggests that the renal involvement in DAS is indistinguishable from NPHP, making it less distinct from the other cerebello-oculo-renal disorders that overlap with JS[24,28,87].

Bardet Biedl Syndrome (BBS)

Bardet–Biedl syndrome (BBS: OMIM 209900) is characterized by obesity, mental retardation, polydactyly, gonadal malformation, retinal dystrophy and renal dysfunction[88-90]. Neurological malformations are unusual, but cerebellar abnormalities have been reported in the literature[91,92] and, in particular, a case of CVH has been documented in a patient with BBS[93]. Although not reported to be

present, we found clear evidence of the MTM in the MRI data for this patient, suggesting a link between BBS and JS. Fourteen genes, namely *BBS1*, BBS2, *ARL6 (BBS3)*, *BBS4*, *BBS5*, *MKKS (BBS6)*, *BBS7*, *TTC8 (BBS8)*, *PTHB1 (BBS9)*, *BBS10*, *TRIM32 (BBS11)*, *BBS12*, *MKS1 (BBS13)*, *CEP290 (BBS14)*, have been identified to date and all of the encoded proteins have been localized to cilia and/or implicated in ciliary function and assembly, including cytoskeletal reorganization and cytokinesis[9,88,94-101]. Furthermore, tandem affinity purification and mass spectroscopic analysis has identified a complex of BBS proteins (termed "BBSome") that is needed to promote ciliogenesis, most likely by mediating vesicular transport to the cilium[102]. It remains to be seen whether other ciliopathic syndromes involve similar processes.

Leber Congenital Amaurosis (LCA)

Clinically, LCA is characterized by severe early visual loss, nystagmus (involuntary oscillation of the eyes), amaurotic pupils (without perceptible lesion), and absent electrical signals on electroretinogram[103]. Fourteen causative genes have been identified to date and explain ~70% of cases[103]. These genes involve diverse structural and functional processes in the retina, but a subset of these genes, *CEP290*[104], *LCA5*[105], *RPGRIP1*[106], and *TULP1*[107], have been implicated in cilia and cilia transport functions overlapping with JS and NPHP. However, manifestation of other features, most frequently mental retardation[103], preclude diagnosis of true LCA and require clinical reclassification; nevertheless, they support a shared mode of disease pathogenesis. Many of these fit within the

Joubert spectrum, in particular, those caused by mutations in *CEP290*[108].This overlap supports a ciliopathic model for a subset of LCA cases.

FUNCTIONAL GENE CANDIDATES

Because the pathology of JS suggests defects of early cerebellar development, particularly of structures derived from the primitive isthmus[109], genes involved in cerebellar patterning at the IsO have been tested as candidate genes, especially those with comparable phenotypes in mouse models. The swaying mouse, which was shown to have a truncation mutation of *Wnt1*, has a phenotype reminiscent of JS, i.e. ataxia, and agenesis of cerebellar structures[110]. Mutant alleles of *Fgf8*, *En1* and *En2* also result in cerebellar abnormalities. A hypomorphic allele of *Fgf8* was shown to cause deletion of midbrain and hindbrain structures[111]. *En1* and *En2* mice also manifest absent or abnormal cerebellar structures[112,113]. Mutations in these genes, however, could not be identified in JS patients screened thus far, suggesting that they are not likely to be a common cause of JS[114,115]. The *ZIC* (zinc fingers in the cerebellum) family of transcription factors was named for its exclusively cerebellar expression in adults. Embryonically, they are more widely distributed and have been implicated in a variety of developmental functions[116,117]. *Zic1* mutant mice have hypoplastic cerebella that are missing anterior lobules of the vermis[118]. They also have behavioral deficits of ataxia and hypotonia, as in patients with JS, and were thought to be a good model for the disease[119]. However, in an analysis of 35 JS pedigrees, *ZIC1* was also excluded as a causative gene[120]. In fact, heterozygous

mutations in *ZIC1* and *ZIC4* have been reported to be a cause of the related, but distinct Dandy–Walker malformation, characterized by hypoplasia and upward rotation of the vermis, cystic enlargement of the fourth ventricle and often hydrocephalus[121].

POSITIONAL CLONING

The lack of success with functional candidate screening suggests that novel genes are involved in JS and that linkage mapping may be more fruitful. In line with this and with the hypothesis of a novel ciliary mechanism for this disease, ten genetic loci have been mapped. Many of these causative genes have been identified, and all of them appear to encode cilia-associated proteins. They are INPP5E[122] (9q34.3, JBTS1: OMIM 213300), 11p12–q13.3[123,124](JBTS2: OMIM 608091) and *AHI1*[125,126] (6q23, JBTS3: 608629), *NPHP1*[35,36] (JBTS4, OMIM 609583), *CEP290*[71,72] (12q21.3, JBTS5: OMIM 610188), *TMEM67*[127] (JBTS6: OMIM 610688), *RPGRIP1L*[128,129] (JBTS7: OMIM 611560), *ARL13B*[130] (3q11.2, JBTS8: OMIM 612291), *CC2D2A/MKS6*[131] (JBTS9: OMIM 612285), *OFD1*[132] (JBTS10: OMIM 300804). Because mutations in these genes only explain an estimated 30-40% of JS cases, there are likely to be many more genes involved.

AHI1

AHI1, the Abelson helper integration 1 gene, was initially identified as a common murine helper provirus integration site[133] and only more recently found

to encode a protein[134]. Jouberin, encoded by *Ahi1*, contains seven WD40 repeats, an SH3 domain, potential SH3 binding sites and an N-terminal coiled–coiled domain. Numerous putative casein kinase, tyrosine kinase and protein kinase C phosphorylation sites can also be detected in the sequence[134]. The mRNA transcript is widely expressed in the brain at a range of time points[125,126]. WD40 domains have been found in proteins involved in a variety of functions including signal transduction, RNA processing, transcriptional regulation, cytoskeleton assembly, vesicle trafficking and cell division[135]. Similarly, SH3 domains are a common feature on signaling molecules, involved in numerous pathways[136]. Consistent with the diversity of cilia functions, recent evidence implicates multiple distinct roles for *AHI1* in disease in addition to classic JS.

Ahi1 and oncogenesis

Though the *Ahi1* locus in mouse was initially thought to serve only as a preferred integration site for a murine helper provirus in the pathogenesis of Abelson murine leukemia virus-induced pre-B-cell lymphoma[133], subsequent studies have supported the idea that disruption of the *Ahi1* gene directly contributes to oncogenesis. Jiang *et. al.* found that this locus encoded Ahi1 trancripts that were upregulated as a result of the provirus insertion[134]. In human leukemic cells, AHI1 is found to be most highly expressed in the most primitive hematopoietic cells and then downregulated during differentiation. In leukemic cells, AHI1 levels were found to be dramatically deregulated, particularly in cutaneous T-cell lymphoma cell lines derived from Sezary patients[137]. Consistent

with this, knockdown of *AHI1* in these cells decreased growth factor independence and tumor promoting activity of these cells[138]. *AHI1* is also upregulated in chronic myeloid leukemia (CML), where it was thought function as a downstream target of BCR-ABL[139]. Regulation of ciliogenesis and cell cycle is likely to be linked due to the shared requirement for centrioles, but how/whether AHI1 fits into this model remains unclear.

Ahi1 and neuropsychiatric disease

Schizophrenia is a complex mental disorder affecting thought and perception and is thought to have a strong genetic component with an estimated 60-80% heritability (OMIM 181500)[140]. Linkage and genome-wide association studies have implicated hundreds of loci, but none have been reliably substantiated. Interestingly, linkage analysis in an inbred Arab-Israeli family, identified a small interval containing the *AHI1* gene as a candidate for schizophrenia[141]. This group further supported this data with an independent analysis in a larger Icelandic cohort, finding a small, but significant effect[142], strengthening the case for AHI1 as a candidate susceptibility locus for schizophrenia. Interestingly, a similar case was made for *AHI1* for association with autism[22,23,143], suggesting broader involvement of *AHI1* in cognitive disorders.

THE CILIA CONNECTION

Cilia and the cerebellum

The current evidence from related diseases and their causative genes suggest a surprising role for cilia in neuronal development. Consistent with this, 9+0 primary cilia have been reported in a large number of cell types in the brain[144-146], including Purkinje and granule cells of the cerebellum, where they are found protruding between extracellular spaces, even during proliferative phases[147,148]. In fact, cilia are present in a majority of vertebrate cells and can be very structurally and functionally heterogeneous.

Evidence is accumulating for the function of primary cilia as flow mechanosensory signaling modules in renal epithelial cells[149,150], but exactly how non-motile primary cilia are functioning in the brain is less clear. Specific receptors have been specifically localized to subpopulations of neuronal cilia, *i.e.* somatostatin receptor 3[151,152] and serotonin receptor 6[153]. It is likely that different populations of neuronal cilia may be specialized to transduce signals, perhaps downstream of morphogens like Wnts or Shh, to regulate proliferation or differentiation. In support of this idea, recent evidence from conditional inactivations of Kif3a, show a requirement for ciliogenesis in aspects of brain development, particularly with regards to Shh signaling[154,155]. Young-Goo *et al*., found that expansion of granule neurons in the dentate gyrus depended on Shh signaling through the primary cilium by studying a neuronal-specifc mouse knockout of *Kif3A* as well as *Ift88* and *Ftm.* Similarly, absence of *Kif3a* and *Ift88* in the cerebellum results in impairment of *Shh*-dependant granule cell precursor proliferation[154,156]. Another study found that adult inactivation of Kif3A showed temporal differences in *Kif3A* requirement[157], *i.e* that late inactivation of Kif3A

resulted in a substantially milder ciliopathy phenotype in the kidney and also obesity that is not observed in early inactivation of *Kif3A*. Further analysis showed that this was due to defective regulation of feeding behavior associated with specific loss of *Kif3A* in the hypothalamus (in pro-opiomelanocortin-expressing cells).

Based on these findings, it is likely that novel ciliopathy-associated proteins such as Jouberin and nephrocystin could be functioning either downstream of cilia-dependant signaling cascades or possibly through IFT mechanisms, bringing necessary structural or signaling components to or from the cilium (Figure 1.3). Indeed, other cilia-associated genes such as inversin have already been implicated in cell cycle and/or transcriptional regulation. It remains to be shown whether *AHI1*, *NPHP1* and other JS genes function similarly.

Photoreceptor cilia trafficking

Retinal photoreceptors are particularly sensitive to perturbation of cilia due to the specialized photoreceptor outer segments (OS), which are the light sensing organelles of the cells. An outer segment, in fact, is a cilium-derived structure consisting of highly structured stacks of membranous disks corresponding to the distal cilium. This is continuous with the connecting cilium, which represents an expanded transition zone together with the basal body[158] that is the “corridor” between the inner and outer segments (Figure 1.4a). A large number of molecules are known to be present within the outer segment and require efficient transport to and (less frequently) from the outer segment both for

development and normal functioning of the OS. Unique to photoreceptor cilia is the continuous phagocytosis and renewal of OS disks, such that OS disk biogenesis is a constant requirement throughout the life of the photoreceptor.

Rhodopsin, in particular is important to the function of the OS as the initial sensor and transducer of light signals, and is abundant in OS disk membranes [159]. In response to light, rhodopsin rapidly undergoes a conformational shift that is critical for triggering the downstream signaling events that lead to hyperpolarization of the cell[160] (Figure 1.4b). In addition to these abundant molecules, a recent study of the photoreceptor proteome identified nearly 1200 different proteins specifically associated with the OS[11]. Despite these large numbers, the direct mechanisms by which these molecules are distributed to the OS are poorly understood.

One prevailing model for trafficking to the OS is movement through the connecting cilium via molecular motors (Figure 1.4c). Consistent with this, mutations in IFT genes have been found to result in retinal degeneration associated with mistrafficking of OS proteins and impaired OS morphogenesis. This was first demonstrated by conditional inactivation of Kif3A in mice by expressing Cre in mature photoreceptors of Kif3A flox/flox mice using the *IRBP* promoter[161]. Inactivation of Kif3A led to accumulation of proteins within the inner segment and specifically, mislocalization of opsin and arrestin, followed by subsequent degeneration of photoreceptors. These results supported an IFT dependant model for opsin transport. Mutations in other components of IFT in mouse and zebrafish models, IFT88, IFT57, IFT172[162-164], have revealed similar

phenotypes of OS structural defects and degeneration, lending further support to this model. A limitation of these studies is the lack of direct evidence for IFT interaction with OS cargo; only recently has biochemical evidence for IFT complexes containing rhodopsin and other important OS proteins been reported[165].

Data on cilia biogenesis in *in vitro* models have also underscored the importance of vesicular targeting/trafficking to the cilium. Considering the enrichment of membrane-associated proteins in the OS, these models are particularly important for the photoreceptor cilium. The majority of the research on photoreceptor vesicular trafficking does not support trafficking of vesicles through the cilium, owing to the clear absence of vesicles in this structure. Rather, a model is emerging whereby vesicles containing necessary transmembrane proteins fuse to the plasma membrane near the base of the cilium, where they subsequently interact with IFT complexes to facilitate transport [161,162]. This process require specific Rab GTPases, including Rab8a, 17, and 23, which have been implicated in ciliogenesis[102,166,167]. Rab8 in particular has been demonstrated to be enriched at the cilium and promotes extension of the ciliary membrane, possibly in cooperation with a BBS complex[102]. Inactivation of Rab8 in *Xenopus* was found to cause IS accumulation of opsin and subsequent cell death of photoreceptors[168].

A competing model was recently proposed whereby vesicles budding from the base of the OS or transported through the cilium are proposed to fuse to nascent outer segment disks forming internally[169]. This directly contrasts to the

prevailing model whereby new disks are formed by the evagination of the membrane at the base of the OS followed by pinching off for disk closure[170]. The validity of this model is unclear as the bulk of the existing data demonstrate open nascent disks consistent with the evagination model and vesicles are not generally observed within cilia or the base of the OS.

CONCLUSIONS

JS is a part of a spectrum of developmental disorders with a complex midbrain–hindbrain malformation as well as involvement of other systems—renal, retinal and/or hepatic. Mutations of *AHI1* have recently been shown to cause a form of JS more penetrant for CNS and retinal involvement, but the function of this gene is largely unknown. However, it is interesting to find that genes associated with related disorders all seem to encode proteins involved in cilia function or assembly, suggesting an interesting link between cilia and neuronal development. It is tempting to speculate that genes involved in JS may also be involved in cilia or in mediating cilia-dependent signals.

ACKNOWLEDGEMENTS

Part of the introduction was published as: Louie, Carrie M; Gleeson, Joseph G. Genetic Basis of Joubert Syndrome and Related Disorders of Cerebellar Development. *Hum Mol Genet,* 14, Spec No. 2, R235-42, 2005. The dissertation author was the primary investigator and author of this paper.

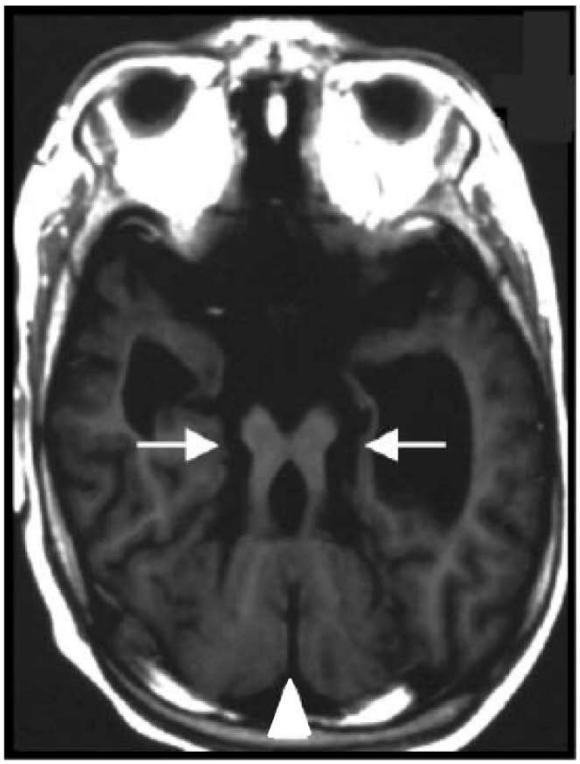

Figure 1.1 Molar tooth sign on radiographic imaging. T1-weighted MRI showing the characteristic “molar tooth” malformation (arrows) and vermis hypoplasia (arrowhead).

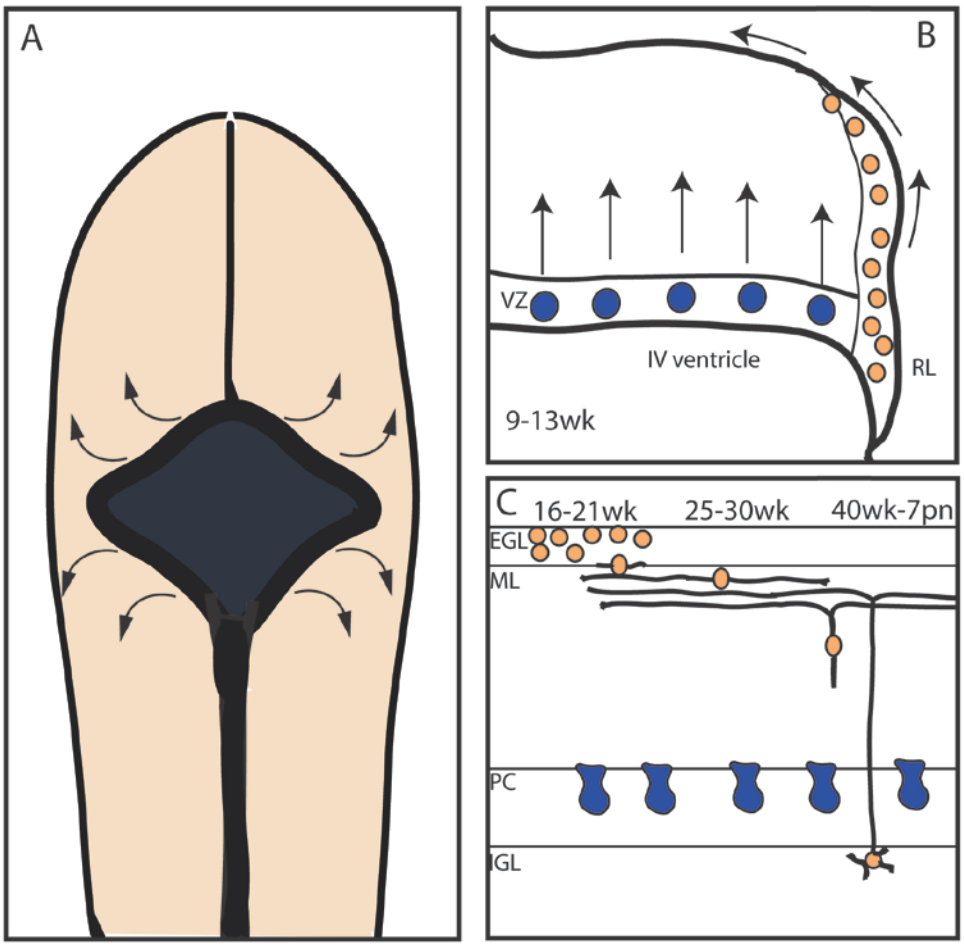

Figure 1.2 Schematic overview of cerebellar development. **(A)** Diagram of dorsal view of cerebellar anlage showing migration from the rhombic lip over the surface of the neural tube. Granule neuron precursors migrate rostrally, while precursors of precerebellar nuclei, migrate ventrally. **(B)** Diagram of cross section through the anlage showing radial migration of Purkinje cell precursors from the ventricular zone (VZ) and tangential migration of granule cells from the rhombic lip (RL). **(C)** "Time-lapse" diagram of granule neuron migration. Granule cell precursors proliferate in the outer EGL. Postmitotic cells move into the inner EGL and extend parallel axons and a descending process prior to migration through the molecular layer (ML) along fibers of Bergman glia (not shown), until settlement in the internal granule layer (IGL).

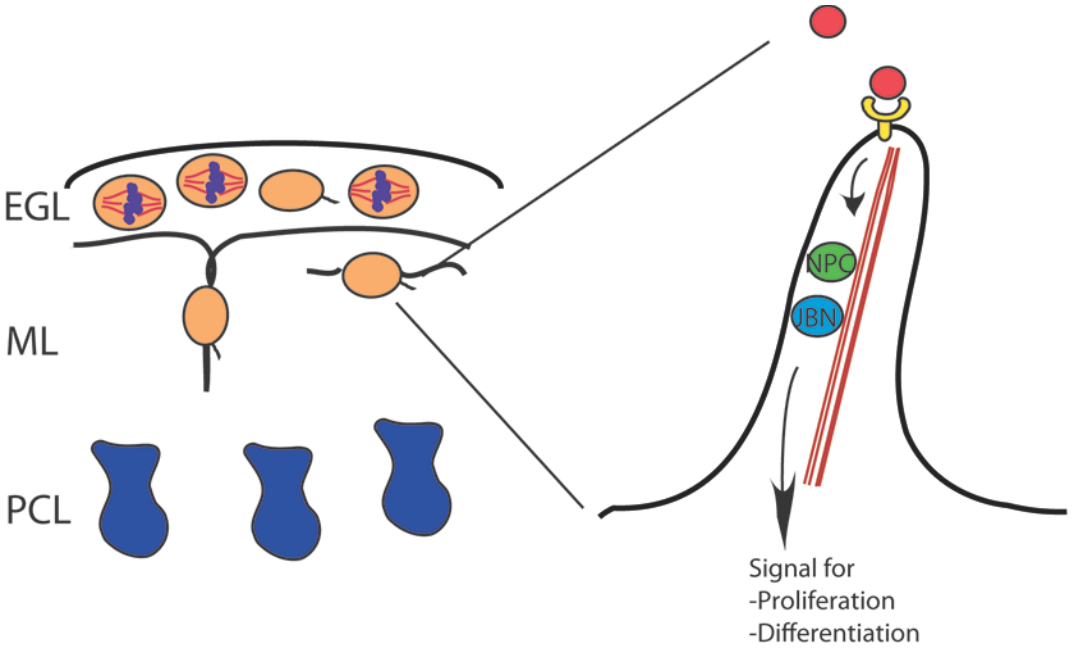

Figure 1.3 Model for cilia-based signaling in cerebellar development and potential role of jouberin (JBN) and nephrocystin (NPC). Cilia are present on most if not all cells of the cerebellum, including cells of the EGL and migrating neurons. JBN and NPC may be required for transduction of morphogenic signals, possibly directly or indirectly through cilia or IFT-based mechanisms, to regulate proliferation or differentiation.

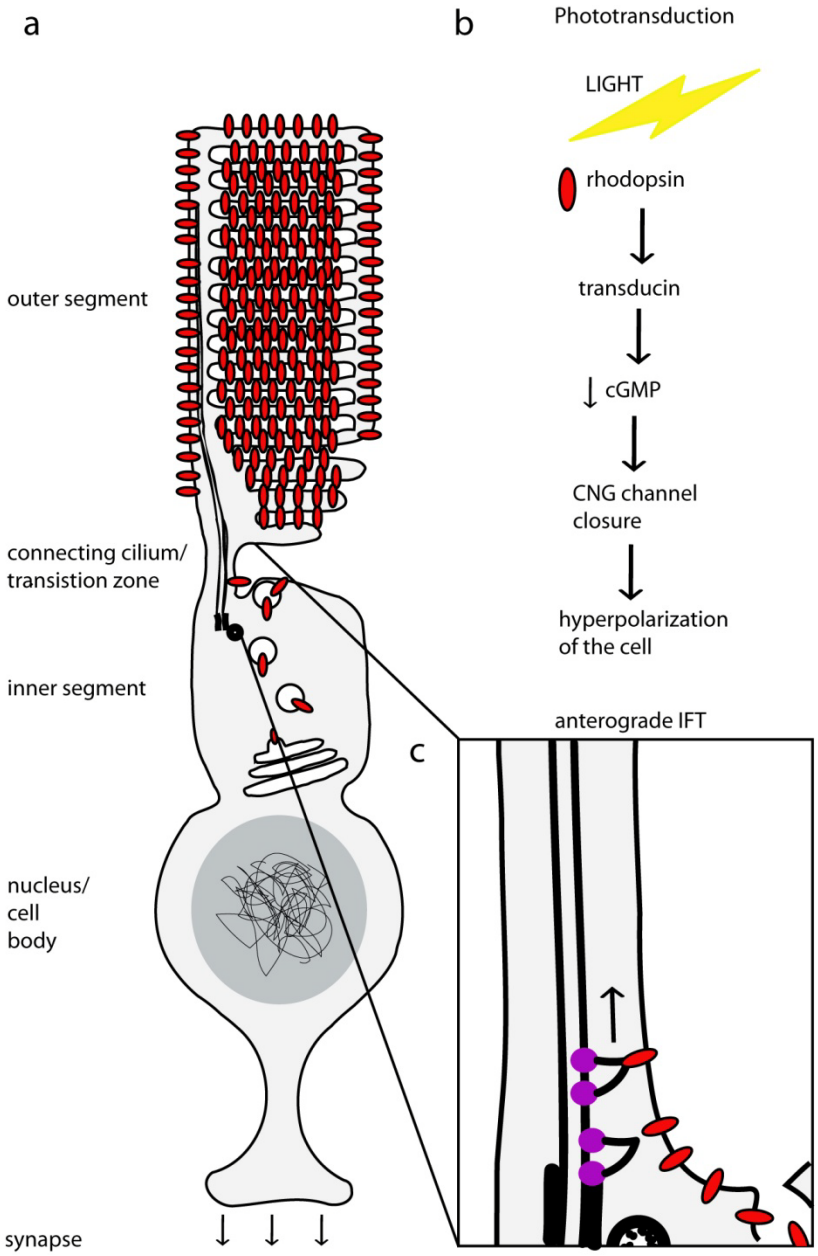

Figure 1.4 Photoreceptor structure, function, and model for intraflagellar trafficking in development and maintenance. **(a)** Schematic of a photoreceptor (not drawn to scale), showing outer segment disks, connecting cilium, inner segment, cell body, and synapse. **(b)** Schematic showing basic events underlying normal phototransduction (c) Model for trafficking of OS membrane components by IFT. Vesicles budding from the ER carrying rhodopsin (and other membrane components of OS) fuse at the base of the cilium. A heterotrimeric complex of kinesin-II and other associated IFTs (not shown) transport along the cilium cargo needed for OS production and maintenance, including rhodopsin.

CHAPTER 2: CHARACTERIZATION OF AHI1 AND GENERATION OF *Ahi1* CONDITIONAL KNOCKOUT MOUSE MODEL

ABSTRACT/SUMMARY

AHI1 was the first gene to be linked and cloned for JS and was a relatively novel gene of little known function. No mouse models of Joubert syndrome had been described and nothing was known about the mechanisms underlying its pathogenesis, making Ahi1 an ideal candidate for study. Using a combination of approaches, I found that *Ahi1* was broadly expressed throughout mouse brains at a range of timepoints. Subcellularly, Ahi1 exhibited dynamic localization patterns in the cytosol and at the base of the primary cilium consistent with the emerging cilia hypothesis for JS. To examine loss of function of *Ahi1* in the mouse model, I inactivated Ahi1 through targeted homologous recombination. Initial results revealed phenotypes in the mouse distinct from human in the absence of the Ahi1 gene, most prominently featuring runting and neonatal lethality with relatively preserved brain morphology. This suggests species- or background-specific effects of *Ahi1* on ciliopathy phenotypes.

RESULTS

AHI1 Expression

Expression patterns of *Ahi1* mRNA transcripts in the mouse were consistent with developmental neural function[125,126], with broad expression in CNS tissues at a range of timepoints[125]. Within the brain, expression in the

cerebellum was relatively low in the mouse, with highest levels in the hypothalamus[126]. To determine the subcellular distribution of AHI1 protein, I stained various cultured immortalized cell lines using a rabbit polyclonal antibody generated to the conserved epitope, c-VKIHVVDEHTGQYVKKDDS. This revealed a dynamic localization pattern that varied depending on cell type and on stage of cell cycle (Figure 2.1). In confluent, ciliated cells, Ahi1 is localized to largely to the cilium as demonstrated by immunofluorescence and by overexpression of GFP-tagged Ahi1 (Figure 2.1a). A small proportion of ciliated, renal epithelial cells also show distribution along cell-cell junctions. In actively dividing cells, Ahi1 is distributed more dynamically throughout the cytosol as puncta and as fibrillar structures partially overlapping with actin (Figure 2.1b). These results suggest dynamic roles for Ahi1 function at the cellular level.

AHI1 germline null mouse model

Mouse and human AHI1 share greater than ~70% sequence identity with particularly high conservation across putative functional domains[171]. As in the human genome, the mouse genome did not present clear *Ahi1* paralogs which could have been functionally redundant. These features make murine *Ahi1* an ideal candidate for study and for targeted knockout.

To make a conditional allele for Ahi1, I generated a construct targeting exons 6 and 7 with flanking loxP sites as discussed in the Methods (Figure 2.2a). This mouse was bred to an early and constitutive Cre (driven by EIIa promoter) to make germline null alleles. Absence of Ahi1 expression was confirmed by Western blotting (Figure 2b). Homozygous null animals (*Ahi1-/-*) were born at

nearly Mendelian ratios, but were apparently runted by as early as postnatal day 2 (P2) and exhibited low survival rates during the neonatal period (Figure 2.2c, d). This was most likely due to impaired feeding as mutants were frequently observed with less milk in their bellies compared to other littermates. Reducing litter size (to reduce competition from wildtype siblings) did not improve survival, suggesting that this may have been due to defects in feeding behavior, though other possible causes are not excluded by this analysis, such as metabolic or respiratory defects.

Histological analysis of postnatal brains of *Ahi1-/-* and *Ahi1+/-* mice showed overall reduced size, but no clear deficit in midline cerebellar structure (Figure 2.3). Closer inspection of cerebellar structure revealed a similar density of granule neurons and organization of the Purkinje cell layer, although the cerebellum was overall smaller in size. Mice were not visibly ataxic and responded comparably to controls in simple tests of motor coordination (righting reflex). Neuronal specific conditional knockout mice (*Ahi1 Nestin Cko*) showed nearly Mendelian ratios at weaning age, suggesting effects outside of the nervous system on survival.

Ahi1 *is not required for decussation of the corticospinal tract*

Another neurological feature of JS is the absence of decussation (midline crossing) of the several axonal tracts. Most intriguing is the absence or disruption of the pyramidal tract (or corticospinal tract) which has been documented to be associated with abnormally bilateral responses to stimuli of the corticospinal

system[62]. To test whether this may be disrupted in this model, biotinylated dextran amine (BDA-anterograde axonal tracer) was stereotactically injected into Nestin-cre conditional Ahi1 mutants (Ahi1 Nes-Cko) at a position in layer V of the cortex corresponding to motor neurons. This permitted the visualization of a subset of the fibers of this track from one side (right hemisphere), accurately defining axonal pathways. This analysis did not identify defects in midline crossing of *Ahi1-/-* CST axons (Figure 2.4).

Ahi1 *is not necessary for the expansion of the EGL*

Granule neurons are by far the most abundant cell type in the cerebellum (and brain overall) and they reach their peak proliferation rates around P5[172]. To determine whether the subtle difference in cerebellar size in the *Ahi1-/-* mouse could be attributed to proliferation defects consistent with previously proposed oncogenic roles for Ahi1, I tested for differences in bromodeoxyuridine (BrdU, thimidine analog) incorporation in granule neurons of the cerebellum at P4. BrdU is incorporated into all cells undergoing S-phase at the time of exposure and thus, is a robust marker of proliferation. Labeling and immunofluorescent detection of BrdU was done both *in vivo* from brain cryosections and *in vitro* from primary cultured neurons. I found that there was no substantial difference in BrdU incorporation at this stage (Figure 2.5).

Ahi1 *is not necessary for cilia formation in the mouse brain*

Defects in cilia structure have been reported in animal models of BBS[101,173]. To test whether this is the case in *Ahi1-/-* mice, I immunostained brain sections from *Ahi1-/-* and *Ahi1+/+* neonatal mice for cilia markers adenylyl cyclase III[174] and Arl13b[130,175] and found that cilia were comparable between these genotypes, suggesting that Ahi1 is not absolutely required for cilia formation (Figure 2.6). From this analysis, it cannot be ruled out that subtle structural defects exist in the *Ahi1-/-* cilia, but this result may be consistent with the lack of a striking morphological defect in the brain.

These results show that important differences exist between human and mouse phenotypes in the absence of the *AHI1* gene, despite the CNS expression pattern of the *Ahi1* transcript. These differences could be due to species-specific differences in Ahi1 function and or effects of genetic background. The cilia localization pattern of the Ahi1 protein, however, supports the cilia hypothesis for JS and suggests that the *Ahi1* knockout mouse may still provide relevant insights into the pathogenesis of this group of diseases.

METHODS

Animal care

Animals were used in compliance with approved Institutional Animal Care and Use Committee protocols of UCSD.

Generation of Ahi1 mutant mice

Ahi1 conditional ("flox") and null allele mice were generated by targeted homologous recombination in accordance with established protocols. The flox region (containing exons 6 and 7), and the short and long homology arms of *Ahi1* were PCR amplified from 129/SvJ genomic DNA (JAX) with primers containing SalI, BamHI, and XhoI restriction sites, respectively, for each arm; PCR products were Topo cloned (Invitrogen, Zero blunt Topo kit according to manufacturer protocols) and screened by sequencing, prior to subcloning into the modified pflox vector[176](J. Marth) containing PGKneobpA for positive selection and also HSV-TK outside of the homology region for negative selection (Figure 2.2a). This was linearized with SbfI and transfected into 129SvJ derived ES cells. G418 and gancyclovir resistant clones were selected and 9 correctly recombined ES clones were identified by Southern blot with two different probes outside of the cloned homology arms (a 5' and a 3' probe). Two clones were injected into C57Bl/6 blastocysts. High percentage chimeras (>90%) were bred to C57Bl/6 for germline transmission and to EIIa-Cre[177] to generate mosaic Cre recombinants. These were then bred to C57Bl/6 to isolate the null allele and a floxed conditional allele. Mice were genotyped by PCR with the following primers in a multiplex reaction: 5'-TGT CTG TGT GTG CTG GGA GA, 5'-CAT TCC AGC CAG ATC ACA AA, 5'-TTC ATC TGT ATT GAG CCA TTG TC, amplifying a 206bp product for the null allele, a 297bp product for the wildtype allele and a 399bp product for the floxed allele.

Protein blotting

Protein blotting was performed on lysates prepared in modified RIPA buffer using the following antibodies: rabbit anti-Ahi1 and mouse anti–α-tubulin (Sigma, T-6074). All antibodies were diluted 1:1,000 in 4% milk. Secondary detection was performed using horseradish peroxidase–conjugated anti-mouse or anti-rabbit antibodies (1:20,000, Zymax) in 4% milk.

Tissue culture

Immortalized cell lines used (IMCD, MDCK, MEFs) were grown in DMEM supplemented with 10% fetal bovine serum and 1% penicillin/streptomycin. For transfection using Lipofactamine 2000 reagent (Invitrogen), cells were seeded at a density of 40% by area into 8-1cm^2-well culture slides in antibiotic-free media and transfected the following day using 800ng total plasmid DNA/well. Cells were washed and fixed with 4% paraformaldehyde 1 or 2 days following transfection.

Culture of primary cerebellar granule neuron precursors

Culture of primary cerebellar neuron (CGN) precursors was performed based on a previously described method[178]. Cerebella of postnatal day 5 (P5) mice were dissected and neurons were dissociated in trypsin and Dnase with trituration by descending bore Pasteur pipets. Cell suspension was separated by centrifugation through a Percoll gradient (35% on 60% Percoll) and the glial fraction remaining at the top interface was removed and discarded. The neuronal fraction was subsequently removed from the 35%/60% interface, resuspended in granule cell medium (DMEM supplemented with BME, horse serum, fetal bovine serum, and penicillin/streptomycin) and plated onto 8-well culture slides

precoated with poly-D lysine. Four hours later, the media was replaced with serum-free media. The following day, BrdU was added to the culture medium and incubated for 24 hours prior to fixation and immunocytochemical staining. Slides were stained for BrdU (1:100, BD Biosciences) to assess proliferation and Hoescht 33342 and phalloidin (1:500, Alexa 594-phalloidin) to mark all neurons.

In vivo BrdU injections.

Brdu was prepared in sterile filtered 0.007M NaOH/0.09% NaCl at 5mg/Ml concentration and injected subcutaneously in P4 mice at 50ug per gram weight of animal. Mice were sacrificed 4 hours later for immunohistochemistry using mouse anti-BrdU.

Histology, immunofluorescence, and microscopy

For tissue fixation, adult animals were perfused transcardially with PBS followed by 4% paraformaldehyde (PFA). Neonatal tissues were dissected and fixed by immersion in 4% PFA, followed by cryoprotection in 10% sucrose/PBS and embedding in 7.5% gelatin/10%sucrose/PBS, or OCT. Sections were prepared on a cryostat (Leica 3350, 10-20μm sections). Nissl (cresyl violet) staining was performed by standard methods for gross assessment of morphology. For immunofluorescence, samples were blocked in 5% normal donkey serum, 1% bovine serum albumin, and 0.1% Triton in PBS for 1 hour. Primary antibodies were incubated in blocking solution at 4C overnight at the following dilutions (Rb anti-AHI1, 1:100; mouse anti-acetylated tubulin, 1:500). Alexafluor dye-conjugatedsecondary antibodies (Invitrogen) were diluted 1:750 in

blocking solution with 1:10,000 dilution of Hoescht 33342 nuclear dye, and incubated with samples for 1 hour. Slides were mounted with Citifluor aqueous mounting medium and sealed.

Fluorescence imaging was performed on a Deltavision RT Deconvolution Microscope using a 100x objective. Brightfield images were acquired on an Olympus MVX10 macroview microscope.

ACKNOWLEDGEMENTS

Part of Chapter Two was published as: Louie, Carrie M; Caridi, Gianluca; Lopes, Vanda S; Brancati, Francesco; Kispert, Andreas; Lancaster, Madeline A; Schlossman, Andrew M; Otto, Edgar A; Leitges, Michael; Hermann-Josef Gröne; Lopez, Irma; Gudiseva, Harini V; O'Toole, John F; Vallespin, Elena; Ayyagari, Radha; Ayuso, Carmen; Cremers, Frans PM; I den Hollander, Anneke; Koenekoop, Robert K; Dallapiccola, Bruno; Ghiggeri, Gian Marco; Hildebrandt, Friedhelm; Valente, Enza Maria; Williams, David S; Gleeson, Joseph G. *AHI1* is required for photoreceptor outer segment development and is a modifier for retinal degeneration in nephronophthisis. *Nature Genetics* vol. 42, p175-180 (2010); advance online publication, 17 Jan 2010 (doi:10.1038/ng.519). The dissertation author was the primary investigator and author of this paper.

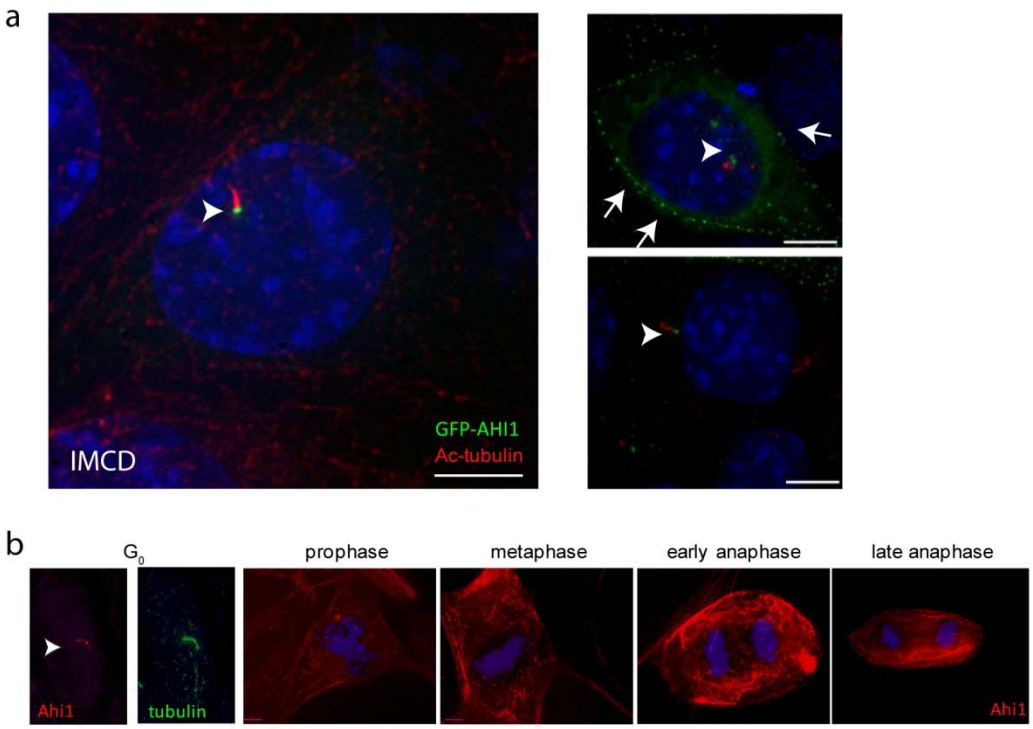

Figure 2.1 Subcellular localization of Ahi1 in cultured cells **(a)** In ciliated cells, GFP-tagged AHI1 localizes consistently to the base of the primary cilium (arrowheads). A subset of transfected cells also exhibit distribution along cell-cell boundaries (arrows), scale=5μm **(b)** Ahi1 immunofluorescence (red) from renal epithelial cells (MDCK) showing cilia localization in confluent cells and fibrillar distribution in dividing cells. Nuclei are indicated by Hoescht 33342.

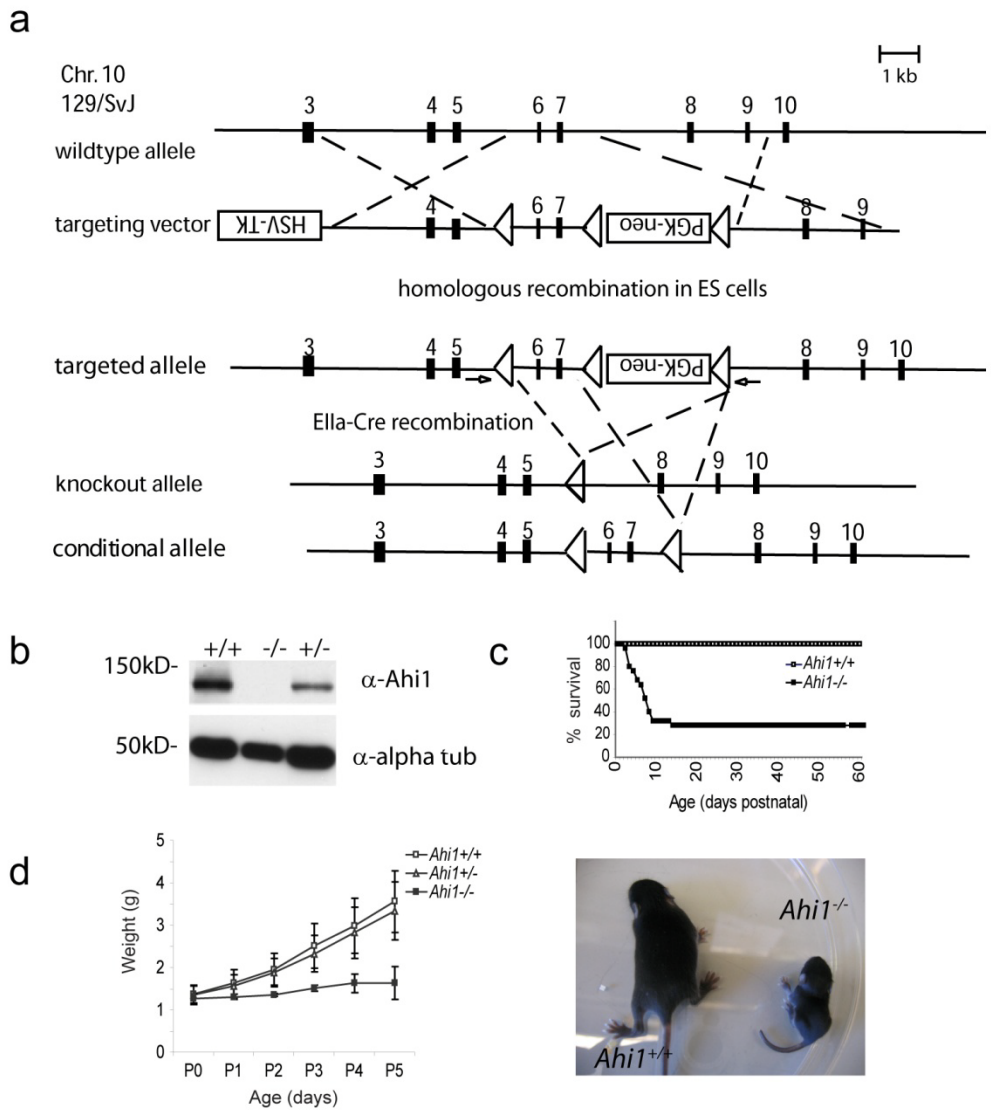

Figure 2.2 Targeting strategy and gross phenotyping of *Ahi1-/-* mice **(a)** The targeting construct was made to introduce loxP sites flanking Ahi1 exons 6 and 7 and flanking homologous Ahi1 sequences for recombination. EIIa-Cre mediated recombination generated mosaics for all possible recombinations, which were then bred further to isolate null and floxed alleles **(b)** Western blotting from *Ahi1+/+, Ahi1+/-* , and *Ahi1-/-* brainstem lysate confirming absence of Ahi1 protein in the knockout and reduced levels in the heterozygote. **(c)** Kaplan Meier plot of survival in *Ahi1-/-* vs *Ahi1+/+* **(d)** weights of *Ahi1+/+, Ahi1+/-* , and *Ahi1-/-* mice plotted over the neonatal period, averaged from 3 litters.

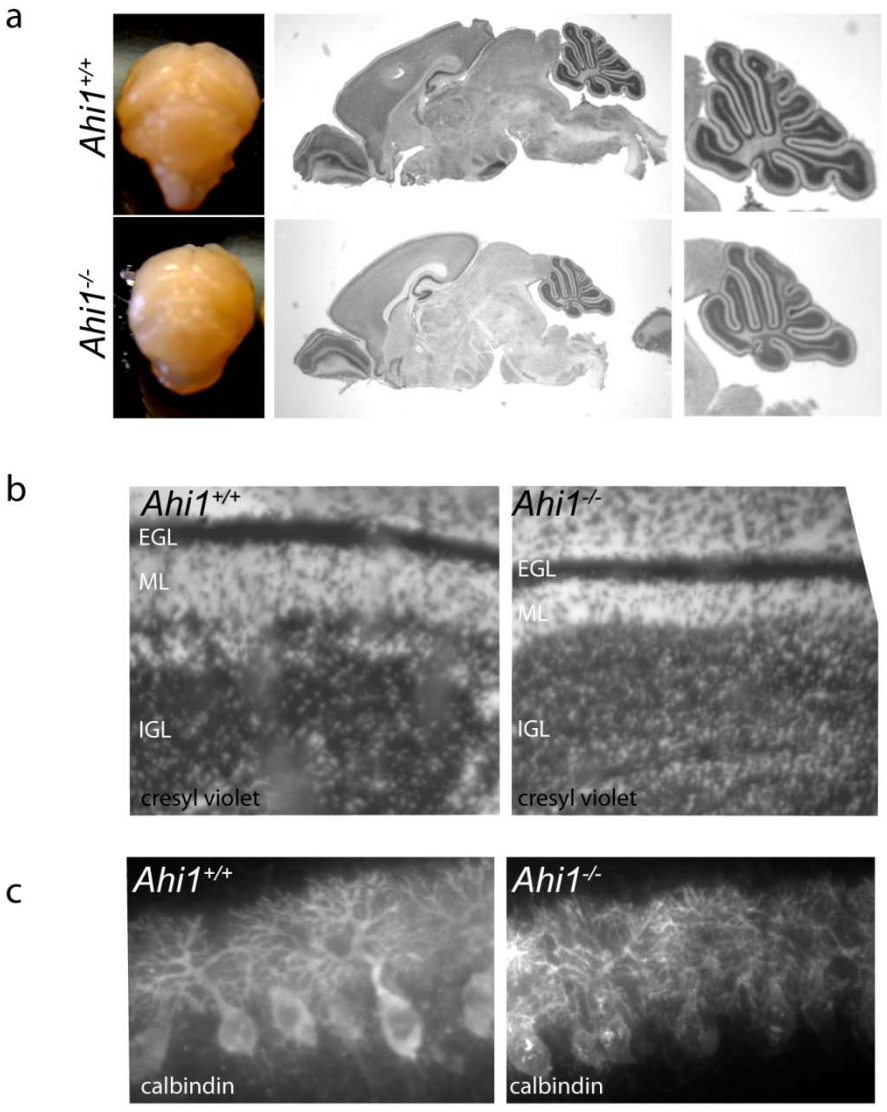

Figure 2.3 Characterization of the *Ahi1* null mouse neonatal cerebellum. **(a)** Whole mount and midline sagittal views of *Ahi1*+/+ and *Ahi1*-/- mice showing reduction in brain and cerebellar size. **(b)** Higher magnification image (10X objective) of comparable regions of cerebellum showing external granule layer (EGL), molecular layer (ML), and internal granule layer (IGL). **(c)** Immunohistochemistry for calbindin D28K labeling Purkinje cells of the cerebellum.

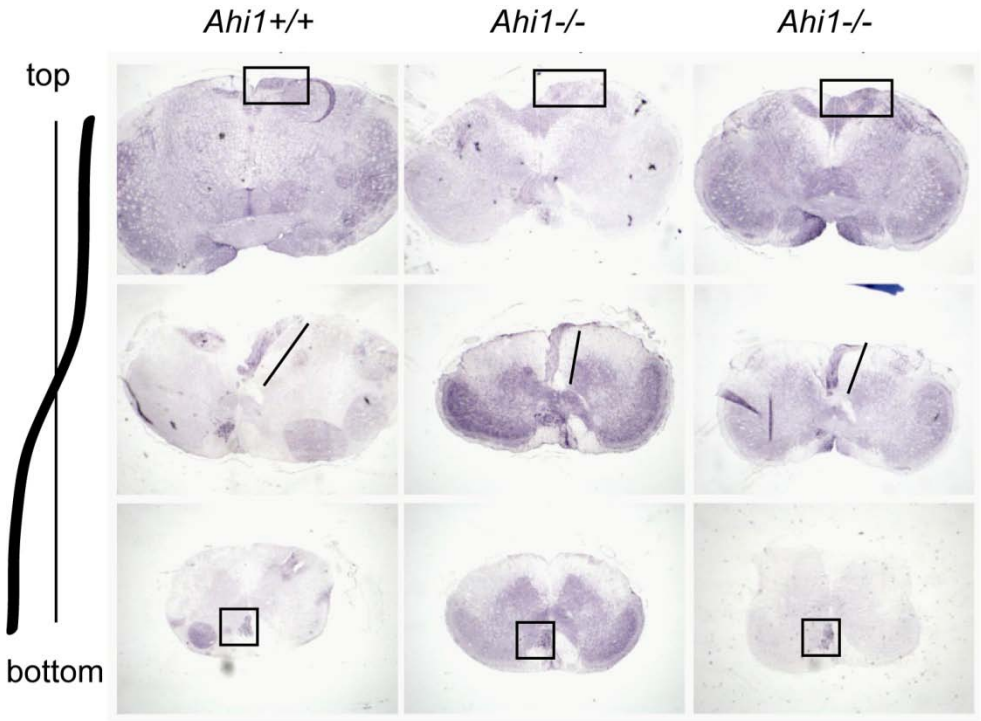

Figure 2.4 *Ahi1* is not required for the decussation of the corticospinal tract (CST). Left: basic schematic of expected path of CST fibers. Panels: DAB-labeled CST fibers descending from the right motor cortex (rectangle in top panels) cross-over at the midline (line in middle panels), and appear on the contralateral side of the spinal cord (box on lower panels). Shown are images from 1 year old mouse spinal cord sections.

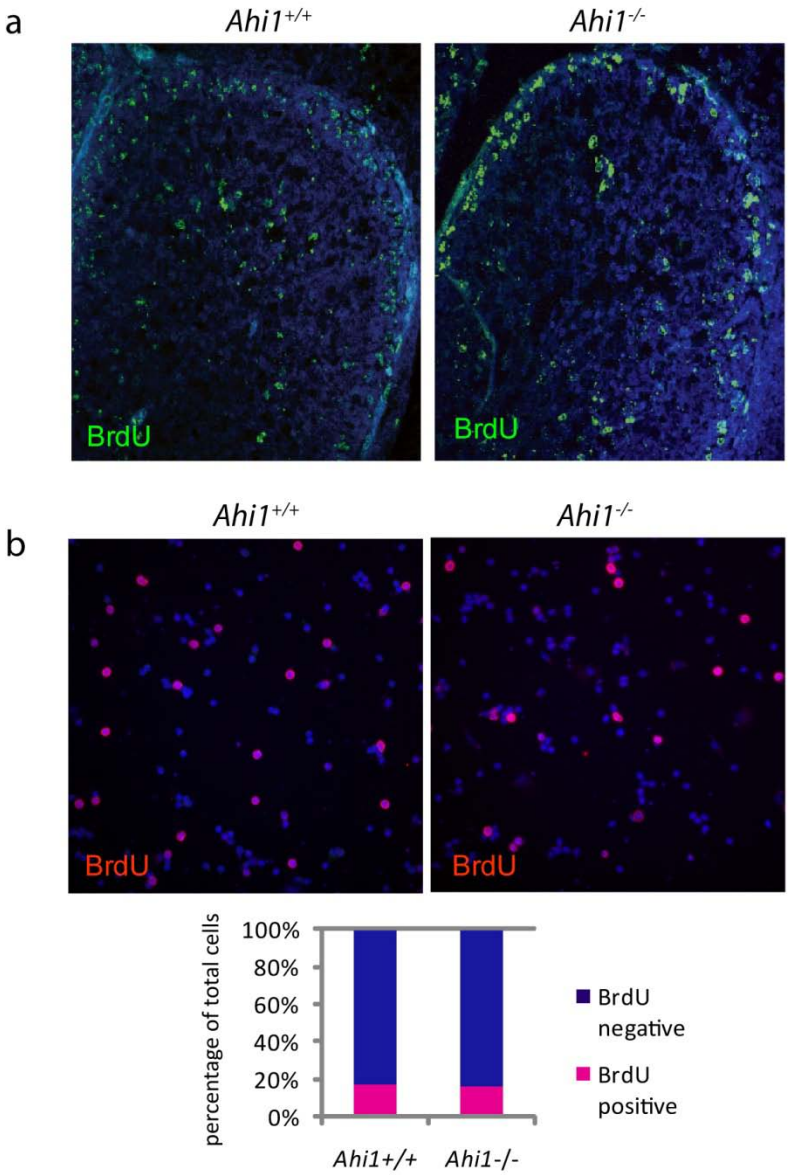

Figure 2.5 *Ahi1* is not required for the expansion of the EGL. **(a)** Midline sagittal sections of P4 *Ahi1*+/+ and *Ahi1*-/- mouse cerebella stained for BrdU following 4-hour BrdU treatment (P4). **(b)** Primary cultures of P4 cerebellar granule neuron precursors stained for BrdU (red) following 24 hour labeling with BrdU. Nuclei are indicated by Hoescht 33342.

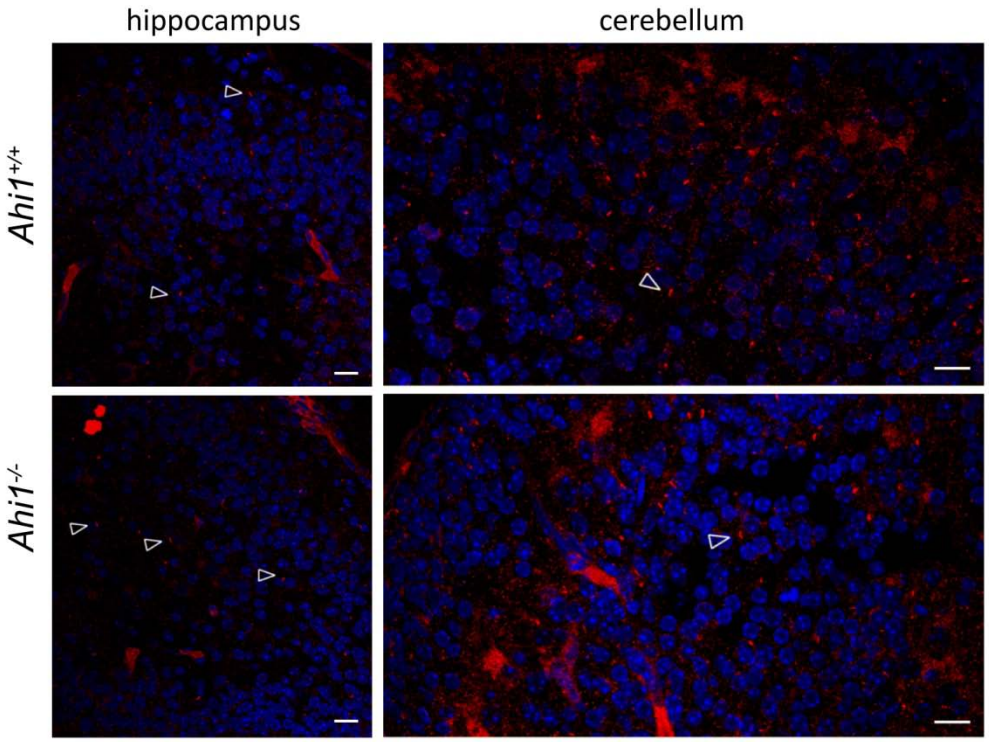

Figure 2.6 *Ahi1* is not essential for ciliogenesis. Sagittal sections from mouse *Ahi1*+/+ and *Ahi1-/-* brains at postnatal day 4 (P4) showing cilia (anti-Arl13b, red, examples indicated by arrowheads) on neurons of the hippocampus and of the cerebellum. Nuclei are indicated by Hoescht 33342 dye, scale=10μm

CHAPTER 3: REQUIREMENT FOR *Ahi1* FOR PHOTORECEPTOR DEVELOPMENT AND SURVIVAL

ABSTRACT/SUMMARY

Degeneration of photoreceptors is a common feature of ciliopathies, owing to the importance of the specialized ciliary structure of these cells. Mutations in *AHI1*, which encodes a cilium-localized protein, have been shown to cause a form of Joubert syndrome that is highly penetrant for retinal degeneration[1,2]. We show that photoreceptors of *Ahi1*-null mice fail to form outer segments and have abnormal distribution of opsin throughout their photoreceptors. Apoptotic cell death of photoreceptors occurs rapidly between 2 and 4 weeks of age in these mice and is significantly (P = 0.00175 and 0.00613) delayed by a reduced dosage of opsin.

RESULTS

Mutations in *AHI1* are identified in 12% of individuals with Joubert syndrome and 20% of individuals with both Joubert syndrome and LCA[1,2,125,126], though *AHI1* mutations are not known to cause nonsyndromic LCA. Furthermore, ~80% of JS patients with AHI1 mutations display LCA-like features. The frequent occurrence of retinopathy in these patients suggests a role for AHI1 in retinal development or function. Consistent with this and the cilia model for Joubert syndrome, we hypothesized that the Ahi1 null mouse would have a retinal defect

consistent with cilia dysfunction. Histological analysis of the retina showed rapid loss of the outer nuclear (photoreceptor) layer, with few nuclei remaining by age 1 month in *Ahi1*$^{-/-}$ mice (Figure 3.1a). As early as postnatal day (P) 10, transmission electron microscopy showed a complete absence of both rod and cone outer segments (specialized disk-shaped membranes of photoreceptor cilia; Figure 3.1b and Figure 3.2a). This far preceded the initiation of apoptotic cell death, which was apparent by ~3 weeks of age as indicated by activated caspase-3 expression (Figure 3.1c). Photoreceptor ciliary axonemes were intact and had normal 9 + 0 microtubule doublet configuration (Figure 3.1b and Figure 3.2b), arguing against a role for *Ahi1* in axonemal development. Dark-adapted electroretinograms (ERG) from *Ahi1* Nestin-Cre Cko and *Ahi1*$^{+/-}$ control mice preceding cell loss confirmed absence of electrical activity (Figure 3.1d). Consistent with its putative role in cilia function, we found that Ahi1 was enriched at the connecting cilium and basal body and overlapped with expression of a *Cetn2* (centrin-2, a centriole–transition zone marker[179,180]) transgene (Figure 3.1e). This expression pattern was reminiscent of those for ciliary transport molecules such as Ift88 (ref. [162]) and other ciliopathy-associated molecules such as Nphp1 (ref.[181]). Together, these results reveal specific defects of outer segment morphogenesis and photoreceptor survival associated with absence of Ahi1.

Rhodopsin (rod opsin and cofactor, retinal), which is responsible for initiating the first steps in light-dependent signal transduction, is also necessary

for outer segment formation[182-185]F. Disruptions of genes required for ciliary transport result in mislocalized opsin and outer segment defects[161,162,165,186], which prompted us to assess opsin localization in *Ahi1*$^{-/-}$ retina. We found severely disturbed opsin distribution as early as P10 (Figure 3.3a). We quantified this in immunogold-labeled sections, which showed significantly increased inner segment labeling in mutants, both in the cytoplasm and particularly along inner segment plasma membranes compared to controls (Figure 3.3b). This difference was ~10-fold for both the inner segment and plasma membrane ($P = 8.0 \times 10^{-6}$ and $P = 2.2 \times 10^{-7}$, respectively). Some other proteins implicated in outer segment morphogenesis appeared grossly intact (Figure 3.2c). We conclude that opsin is significantly misaccumulated in *Ahi1*$^{-/-}$ mice at an early stage of outer segment morphogenesis.

To further test for cell-type–specific requirements for Ahi1 in opsin distribution, we used *Ahi1*$^{flox/flox}$ mice in a series of retinal *in vivo* electroporation experiments performed at P0 (Figure 3.4a). The pCAG-Cre:GFP vector drives Cre:GFP under the constitutive CMV early enhancer/chicken β-actin promoter and was used with the CALNL-pDsRed recombination reporter[187,188]. Photoreceptors with evidence of Cre recombination based upon expression of DsRed also showed recapitulation of the opsin redistribution phenotype by age 1 month (Figure 3.4b), indicating a requirement for Ahi1 in photoreceptors. To test for temporal-specific requirements for Ahi1, these experiments were repeated using the vector pCAG-ERT2CreERT2, which activates Cre under control of 4-

hydroxytamoxifen (4-OHT)[188]. Following 4-OHT dosage at P14, after the peak of outer segment development, we did not detect opsin accumulation at 2 and 4 weeks after Cre induction, despite evidence of recombination based upon expression of DsRed (*n* = 2, Figure 3.4c,d). We conclude that Ahi1 shows temporal specificity in its function in photoreceptors, possibly akin to the time dependence reported for ciliary transport machinery in kidney phenotypes[157]. These data also suggest that other factors might contribute to outer segment developmental defects in this model.

Mislocalized opsin is frequently associated with retinal degeneration in animal models[103,186] and has been indicated as a major cause of photoreceptor cell death in the absence of heterotrimeric kinesin-2 function (D. Jimeno, V.S. Lopes, K. Khanobdee, X. Song, B. Chen, S. Nusinowitz *et al*., unpublished data). Because of the striking accumulation of opsin in *Ahi1*$^{-/-}$ mice, we hypothesized that this might similarly contribute to cell death in *Ahi1*$^{-/-}$ photoreceptors. To test this directly, we reduced opsin levels in *Ahi1*$^{-/-}$ mice by introducing a *Rho* (rod opsin)-null allele[15] into the *Ahi1*$^{-/-}$ background. *Rho*$^{+/-}$ photoreceptors have approximately 40%–50% reduction in opsin content[183,189]. Reduction in opsin dosage did not affect outer segment formation, with similar absence of outer segments in *Ahi1*$^{-/-}$*Rho*$^{+/-}$ compared to *Ahi1*$^{-/-}$ mice (Figure 3.5), but it significantly delayed the cell loss seen in *Ahi1*$^{-/-}$ mice. We found nearly complete rescue of cell numbers at 3 weeks of age (*n* = 3–7, *P* = 0.00175) and partial rescue at 1 month (Figure 3.6; *n* = 3–4, *P* = 0.00613). These data support the

hypothesis that abnormal accumulation of opsin contributes to the loss of *Ahi1*$^{-/-}$ photoreceptors.

METHODS

Animal care.

Animals were used in compliance with approved Institutional Animal Care and Use Committee protocols of UCSD.

Generation of Ahi1 *mutant mice.*

Ahi1 conditional (*loxP*-flanked, 'flox') and null allele mice were generated by targeted homologous recombination. The floxed region (containing exons 6–7), short arm, and long arms of *Ahi1* were PCR-amplified from 129/SvJ genomic DNA (Jackson Labs), flanked with SalI, BamHI and XhoI restriction sites, repectively. These were subcloned into the modified pflox vector[176] (J. Marth) containing PGKneobpA (positive selection) and HSV-TK (outside of homology arms for negative selection). This was linearized with SbfI and transfected into 129SvJ-derived ES cells. G418- and gancyclovir-resistant clones were selected, nine correctly recombined ES clones were identified by DNA blot with two distinct probes (one each at the 5' and 3' ends of the insert), and two clones were injected into C57Bl/6 blastocysts. High-percentage chimeras were bred to C57Bl/6 for germline transmission and to EIIa-Cre to generate mosaic Cre recombinants. Mosaics were bred to C57Bl/6 to isolate null and conditional alleles. Mice were genotyped by PCR in a multiplex reaction, amplifying a 206-bp

(null allele), a 297-bp (wild-type) and/or a 399-bp (conditional allele) product (Supplementary Table 1).

Additional mouse lines.

Rhodopsin-null mice were obtained from J. Lem[183]. The following transgenic mouse lines were used: EIIa-Cre[177], Nestin-Cre (Jackson Labs 003771)[190], Pax6α-Cre[191]and GFP-Centrin2[179]. *Ahi1* alleles were denoted as follows: $Ahi1^{-/-}$ and $Ahi1^{+/-}$ (represents *Ahi1* homozygous germline null and germline heterozygotes, which were used for all experiments except where indicated otherwise), *Ahi1* Nestin-Cre Cko ($Ahi1^{flox/-}$ Nestin-Cre positive; used for ERGs) and *Ahi1* Pax6α-Cre Cko (represents $Ahi1^{flox/-}$ Pax6α Cre^{+}, which were used for generating double mutants with *Nphp1* and only more peripheral regions of retina were analyzed). All animals were from mixed backgrounds (C57Bl/6, SvJ129, 129/Ola) and were compared to littermate or age-matched sibling controls.

Dark-adapted ERG.

Mice were tested using previously described methods[192]. Mice dark-adapted overnight were kept under low red lighting and anesthetized by intraperitoneal injection (10 mg/ml ketamine, 1 mg/ml xylazine at 0.1 ml per 10 g body weight), dilated with phenylephrine HCl and tropicamide and kept on a warm pad. Gold loop electrodes on the cornea were referenced to needle electrodes under the cheek and electrodes clipped to ears served as grounds. Responses were elicited by high-intensity flashes (averaged over $n = 5$) at 1-s

intervals over a time base of 500 ms in a Ganzfeld dome with a photostimulator (Model PS22, Grass instrument company).

Antibodies and fluorescence microscopy.

Mice were anesthetized by isoflurane inhalation and perfused, or eyes were immersed in 4% paraformaldehyde/PBS. 10–25-µm cryosections corresponding to a medial position (intersecting optic nerve) were stained for immunofluorescence per standard protocols except where noted. We used the following primary antibodies: rabbit anti-Ahi1[193] (1:250, after antigen retrieval by microwaving slides for 15 min in 10 Mm sodium citrate, Ph 6.0), mouse anti-acetylated tubulin (Zymed, 6-11B-1, 1:1,000), rabbit anti-RPGR (T. Li, 1:1,000 on barely fixed tissues as previously described)[194], chicken anti-RP1[195] (1:2,000, E.A. Pierce) and mouse anti-opsin (1:250, Chemicon). We used Alexa Fluor dye-conjugated secondary antibodies (1:750, Invitrogen/Molecular Probes) and Hoechst 33342 (1:10,000) nuclear dye. Images were obtained on a Fluoview1000 Spectral Deconvolution Confocal microscope (Olympus), under the same parameters for each experiment.

Histology and electron microscopy.

For conventional electron microscopy (EM), samples were fixed with 2% paraformaldehyde/2% glutaraldehyde/0.1 M cacodylate buffer and embedded in propylene oxide:Epon 812 resin. Semi-thin (0.7 µm) sections were stained with toluidine blue (0.25% toluidine blue with 0.25% sodium borate in water) for light microscopy. Ultrathin sections (70 nm) for electron microscopy were collected on

copper grids and stained with saturated uranyl acetate and lead citrate solution before being imaged on a Phillips electron microscope (model 208).

For immunoelectron microscopy, mice were perfused with 4% paraformaldehyde and samples were immersed overnight in 0.1% glutaraldehyde/4% paraformaldehyde/0.1 M cacodylate buffer and embedded in LR White resin (EMS). 70-nm sections were etched with saturated sodium periodate and blocked with 4% bovine serum albumin. Sections were incubated with anti-opsin (1D4) primary antibody and with goat anti-rabbit IgG secondary conjugated to 12-nm gold (EMS). Sections were subjected to osmium vapor and stained with uranyl acetate and lead citrate. Negative control sections were processed simultaneously and included sections not incubated with primary antibody. Cilia were randomly selected for imaging on a transmission EM microscope (Zeiss).

In vivo *electroporation and 4-OHT treatment.*

Retinal *in vivo* electroporation at P0 was performed as previously described[187,188] using 5 μg/μl total plasmid DNA with 0.01% Fast Green tracer at 0.5 μl/eye at the following mass ratios: pCAG-Cre:GFP/pCALNL-DsRed (1:1), and pCAG-ERT2CreERT2/pCALNL-DsRed/pCX-EGFP (2:1:1), but with a modification: DNA solutions were injected through glass micropipets pulled from capillary tubes (World Precision Instruments, TW150F-3). Plasmids were from C. Cepko through Addgene. For ERT2Cre induction, 4-OHT (Sigma, H7904) was

prepared in corn oil (Sigma, C8267) at 2 mg/ml and was IP-injected (400 µl in a 2-week-old mouse).

Statistics.

Data were expressed as means ± s.e.m. Two-tailed *P* values were calculated by Student's *t*-test. Values <0.05 were considered statistically significant for all tests.

URLs.

Fisher's exact test, http://www.langsrud.com/fisher.htm; risk and confidence intervals, http://statpages.org/ctab2x2.html.

ACKNOWLEDGEMENTS

We thank K. Siever and K. Teofilo for assistance with histology; G. Silva, L. Cheng and M. Davidson for assistance with ERG testing; A. Avila for assistance with clinical data and selecting controls; J. Lem, G. Lemke, T. Burstyn-Cohen and A. Wynshaw-Boris for sharing mice and for feedback and suggestions; K. Zhang, L. Goldstein and B. Zheng for feedback and suggestions; T. Li and E. Pierce for sharing antibodies; C.-H. Sung for sharing rhodopsin plasmid; J. Kim and V. Cantagrel for technical advice; and J. Meerloo with the University of California at San Diego (UCSD) Neurosciences Microscopy Shared Facility (NINDS P30NS047101) for microscopy services and support. This work was supported by the US National Institutes of Health R01NS048453 (J.G.G.),

R01DK068306 (F.H.), P30NS047101 (J.G.G.), F31NS059281 (C.M.L.), R01EY007042 (D.S.W.), UCSD Genetics Training Program institutional training grant T32 GM008666 from the National Institute for General Medical Sciences (C.M.L. and M.A.L), GP08145 grant from Telethon-Italy (E.M.V.) and the Burroughs Wellcome Fund (J.G.G.). D.S.W. is a Jules and Doris Stein RPB Professor. J.G.G. and F.H. are investigators of the Howard Hughes Medical Institute.

Work in Chapter 3 was published as: Louie, Carrie M; Caridi, Gianluca; Lopes, Vanda S; Brancati, Francesco; Kispert, Andreas; Lancaster, Madeline A; Schlossman, Andrew M; Otto, Edgar A; Leitges, Michael; Hermann-Josef Gröne; Lopez, Irma; Gudiseva, Harini V; O'Toole, John F; Vallespin, Elena; Ayyagari, Radha; Ayuso, Carmen; Cremers, Frans PM; I den Hollander, Anneke; Koenekoop, Robert K; Dallapiccola, Bruno; Ghiggeri, Gian Marco; Hildebrandt, Friedhelm; Valente, Enza Maria; Williams, David S; Gleeson, Joseph G. *AHI1* is required for photoreceptor outer segment development and is a modifier for retinal degeneration in nephronophthisis. *Nature Genetics* vol. 42, p175-180 (2010); advance online publication, 17 Jan 2010 (doi:10.1038/ng.519). The dissertation author was the primary investigator and author of this paper.

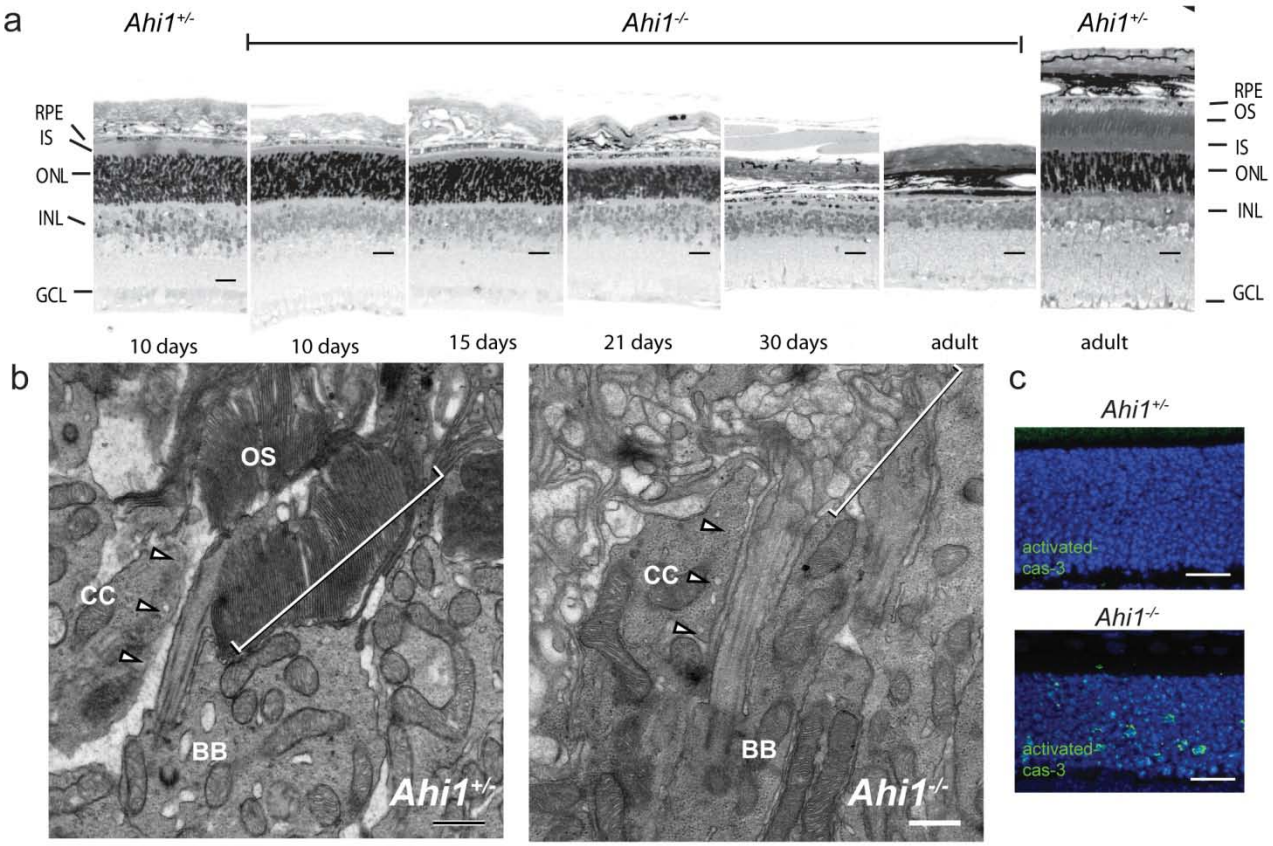

Figure 3.1 Degeneration of photoreceptor cells following failed outer segment development in *Ahi1−L* mouse retina. **(a)** Semi-thin sections of retina stained with toluidine blue from P10 to adult (10 weeks) showing acute loss of the outer nuclear layer (ONL) between P21 and P30. Scale bar, 20 µm. **(b)** Transmission electron microscopy from P10. Outer segments (OS, brackets) are present in *Ahi1+/* but not in *Ahi1−L* mice. Connecting cilia (CC, arrowheads) are present in both. Scale bar, 0.5 µm. **(c)** Photoreceptor cell death is evident before 3 weeks of age, indicated by activated caspase-3 immunofluorescence (green) from 20-µm cryosections. Nuclei are stained with Hoechst 33342 (blue). Shown are representative images from P19 mice. Scale bar, 20 µm.

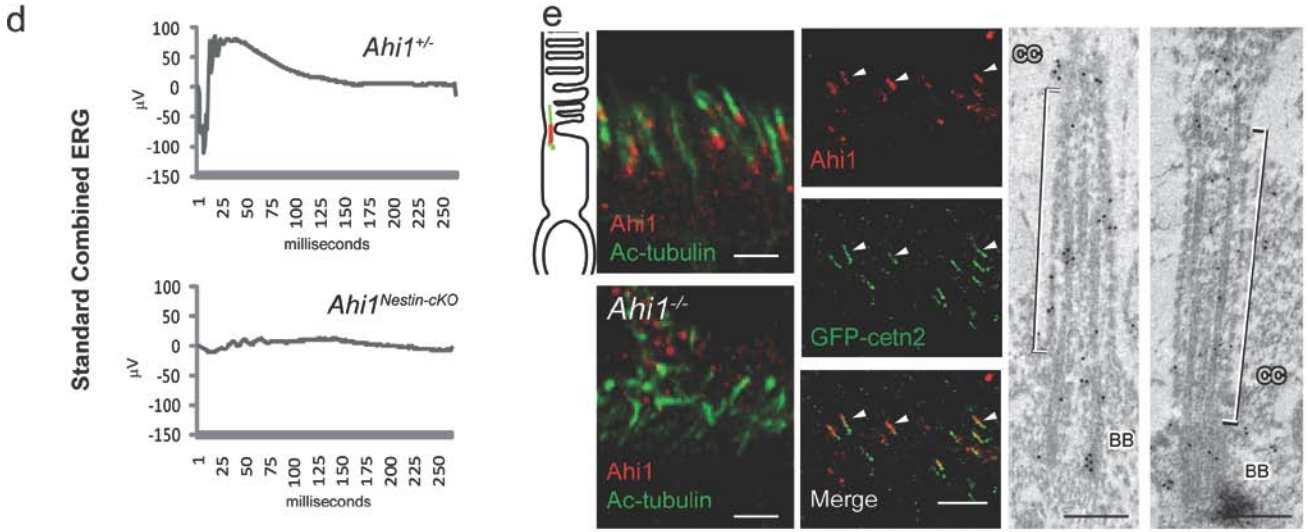

Figure 3.1, continued **(d)** Full-field dark-adapted electroretinograms (ERGs) from P19 *Ahi1*flox/- Cre+ with (*Ahi1*Nestin-cKO) and *Ahi1* heterozygous control mice. Shown are representative waveforms from *n* = 3 or 4 mice per genotype. **(e)** Endogenous Ahi1 localization (red) to the base of photoreceptor-connecting cilium (acetylated tubulin: green) in *Ahi1*+/- Nestin-cKO and *Ahi1*−/− mice. Ahi1 distribution overlaps with centrin-2 (green) in GFP–Cetn-2 transgenic mouse retina. Arrowheads indicating example of GFP–Cetn-2–labeled connecting cilia in 10-μm cryosections. Scale bar, 5 μm. Ahi1 immunoelectron microscopy from P10 retina, showing particles at the basal body (BB) and along the cilium (CC). Scale bar, 0.25 μm.

- section is absent in

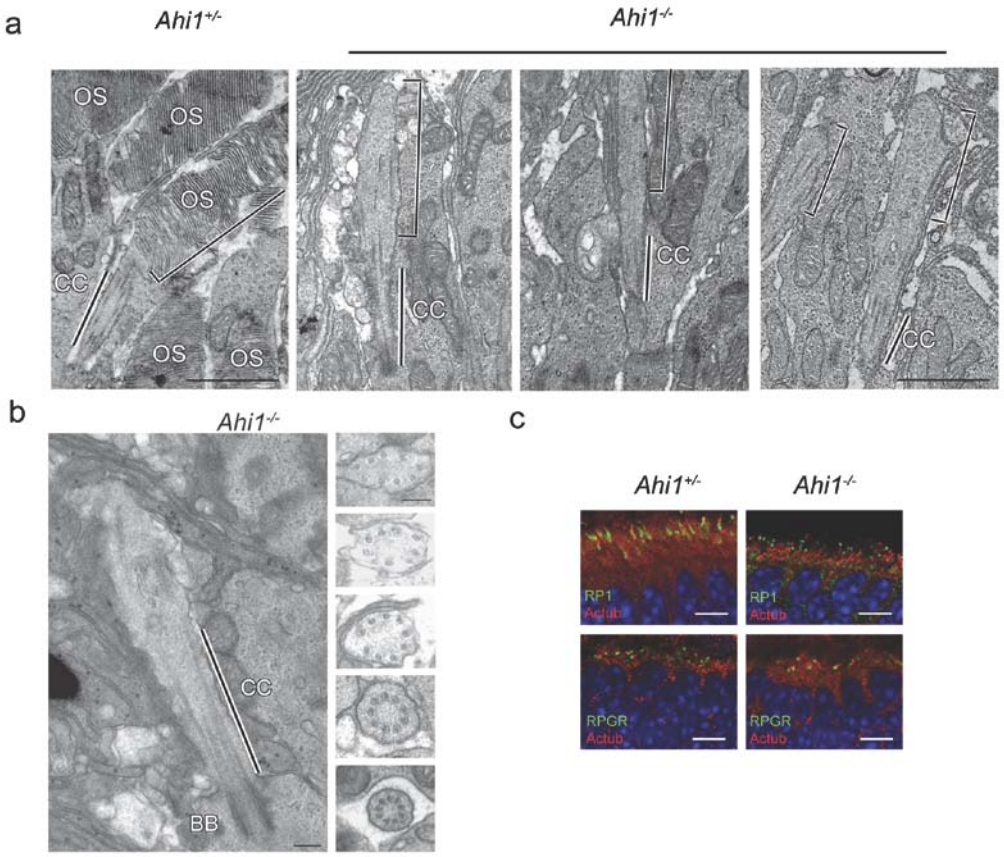

Figure 3.2 Absence of outer segments with relatively preserved axonemes and maintenance of RPGR and RP1 axonemal localization in *Ahi1-/-* mice. **(a)** EM longitudinal views of representative Ahi1+/- control and multiple *Ahi1-/-* photoreceptor cilia demonstrating absence of outer segment disks. OS=outer segments, CC=connecting cilium (and indicated by black lines), brackets indicate OS in control and disorganized membranes in the *Ahi1-/-*, scale=1μm **(b)** longitudinal and cross section views of connecting cilia from *Ahi1-/-* photoreceptors showing axoneme and 9+0 arrangement of microtubule doublets. CC=connecting cilium, BB= basal body. Scale=0.1μm **(c)** Immunofluorescence for RP1 and RPGR (green), acetylated-tubulin (red), and nuclei (Hoescht 33342, blue) from 10μm cryosections of P8 retina, scale=5μm

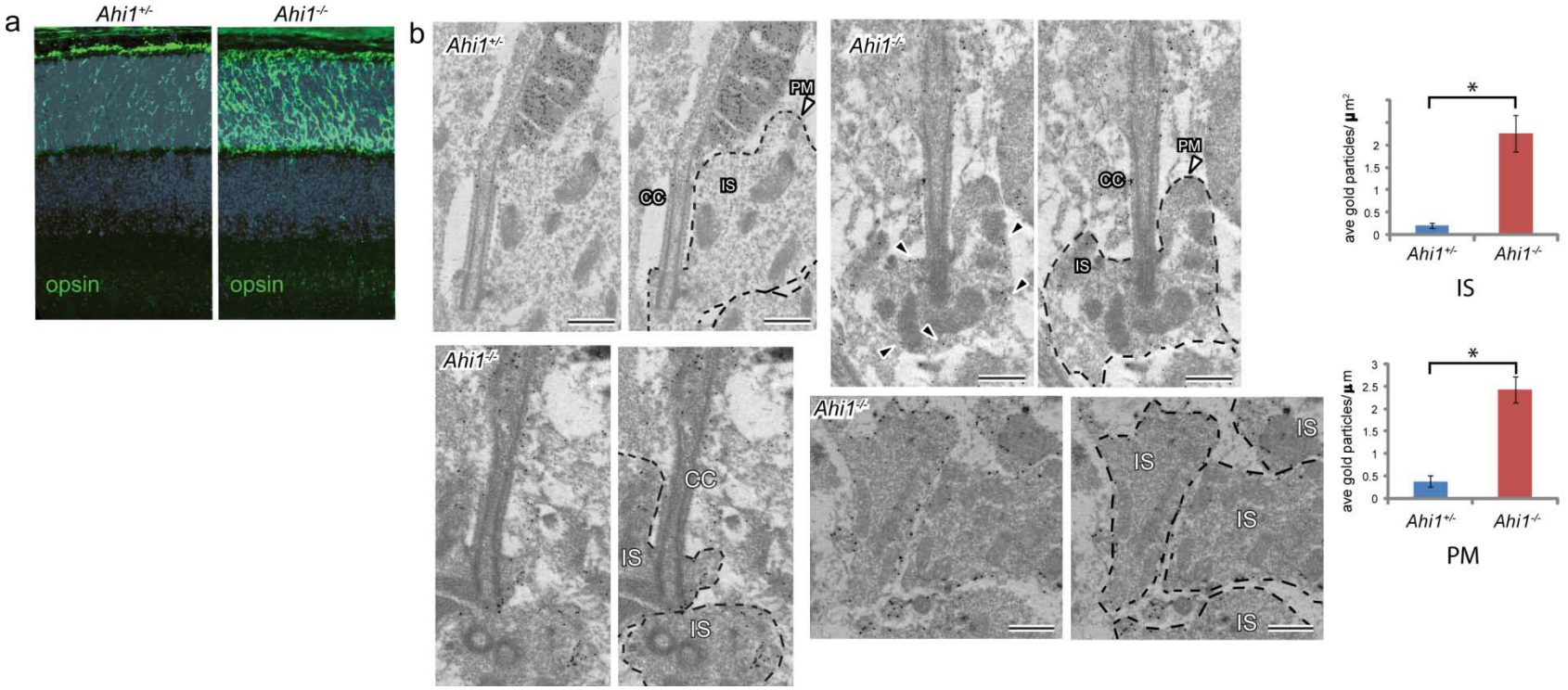

Figure 3.3 Opsin accumulation in *Ahi1-/-* photoreceptors **(a)** Opsin immunofluorescence (green) at P10 in *Ahi1+/* and *Ahi1−/−* retina from cryosections. Nuclei are stained with Hoechst 33342. Scale bar, 20 μm. **(b)** Opsin immunoelectron microscopy and quantification of immunogold labeling from ultrathin sections of P10 *Ahi1+/* and *Ahi1−/−* retina; *n* = 20–23 photoreceptor connecting cilia per genotype. Data are expressed as number of gold particles per μm2 area within the inner segment (IS, defined as within inner segment and at least 30 nm away from plasma membrane, PM; *P* = 8.0 × 10−6), and as number of particles per μm length of inner segment membranes (PM, dashed lines, *P* = 2.2 × 10−7). Black arrowheads indicate examples of abnormally localized opsin; CC, connecting cilium. Scale bar, 0.5 μm. Error bars, s.e.m.

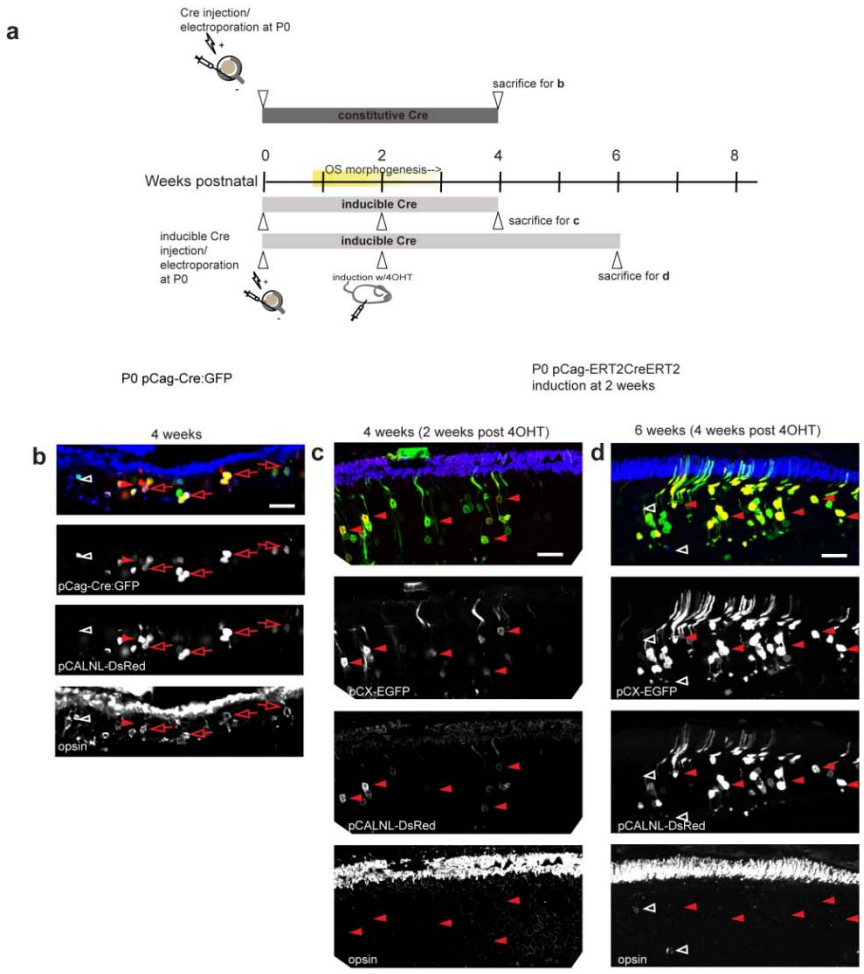

Figure 3.4 Spatial and temporal requirement for *Ahi1* in opsin distribution **(a)** Schematic overview of Cre electroporation experiments showing timing of electroporation, induction, and sacrifice for parts b, c, d. **(b)** Immunofluorescence for opsin (blue) in 25□m cryosections from 4 week old*Ahi1*$^{flox/flox}$ mice electroporated with pCAG-Cre:GFP and pCALNL-DsRed at P0. Red arrows indicating cells positive for Cre (green), Cre reporter(red) and mislocalized opsin (blue); white open arrowheads indicating rare instance of opsin mislocalization in the absence of Cre reporter signal; red arrowhead indicating rare instance of Cre or Cre reporter signal without evidence of opsin mislocalization **(c)** Immunofluorescence for opsin in sections from 4 week old *Ahi1*$^{flox/flox}$ mice electroporated with pCAG-ERT2CreERT2, pCALNL-DsRed, and pCX-EGFP at P0, and induced at 2 weeks. Red arrowheads indicating transfected cells with Cre reporter activity, without evidence of mislocalized opsin **(d)** Immunofluorescence for opsin in sections from 6 week old *Ahi1*$^{flox/flox}$ mice electroporated with pCAG-ERT2CreERT2, pCALNL-DsRed, and pCX-EGFP at P0, and induced at 2 weeks. Red arrowheads indicating transfected cells with Cre reporter activity, without evidence of mislocalized opsin, white arrowheads indicating rare instances of opsin redistribution without evidence of Cre activity. Scale=20μm for all

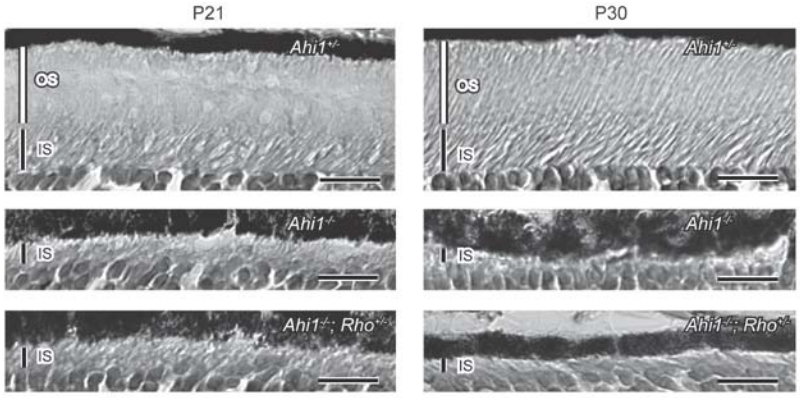

Figure 3.5 Outer segments fail to form on *Ahi1*$^{-/-}$ and on *Ahi1*$^{-/-}$; *Rho*$^{+/-}$ photoreceptors. Ten micron cryosections stained with hematoxylin and eosin and imaged with a 60X objective with differential interference contrast (DIC), from *Ahi1*$^{+/-}$, *Ahi1*$^{-/-}$ and *Ahi1*$^{-/-}$; *Rho*$^{+/-}$ samples at P21 and P30. OS= outer segment, IS= inner segment, scale= 10μm

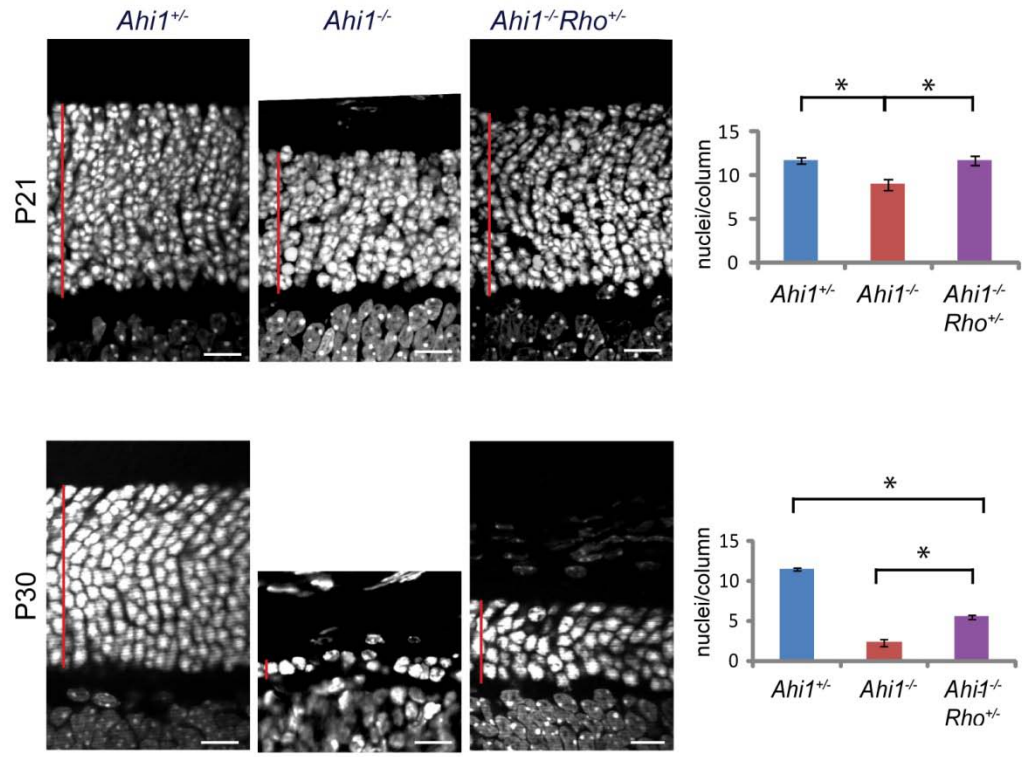

Figure 3.6 Opsin contributes to cell death in *Ahi1*$^{-/-}$ mice. 10 μm cryosections from P21 and P30 retina showing delay of cell loss associated with reduced opsin dosage (*Ahi1*$^{-/-}$*Rho*$^{+/-}$), measured as average number of cells per column (nuclei were stained with Hoechst 33342 and counts are expressed as the average of three counts across each section). Asterisk in top panel denotes significant difference from both control and rescue; n = 3–7, P = 0.00175 (P21) and 0.00613 (P30). Scale bar, 10 μm. Error bars, s.e.m.

CHAPTER 4: ROLE OF MODIFIER EFFECTS ON RETINAL PHENOTYPES IN CILIOPATHIES

ABSTRACT/SUMMARY

Growing evidence supports roles of genetic modifiers on the phenotypic variability of ciliopathies. The strong retinal phenotype of the Ahi1-null mouse suggests that mutations in Ahi1 could affect retinal phenotypes in the context of mutations in related genes. Our results show that, in mouse, the retinal degeneration phenotype shows dosage-sensitive genetic interactions with *Nphp1*, another ciliopathy-related gene. Although it is not a primary cause of retinal blindness in humans, we show that an allele of *AHI1* is associated with a more than sevenfold increase in relative risk of retinal degeneration within a cohort of individuals with the hereditary kidney disease nephronophthisis. Our data support context-specific roles for *AHI1* as a contributor to retinopathy and show that *AHI1* may explain a proportion of the variability in retinal phenotypes observed in nephronophthisis.

Ciliopathies comprise an increasingly diverse group of genetic disorders, unified by their connection to dysfunction of the primary cilium and/or its associated basal body[3]. Because of the pervasiveness of this organelle, these disorders manifest in numerous organs. Joubert syndrome (characterized by cerebellar hypoplasia), Leber's congenital amaurosis (LCA, characterized by

congenital retinal blindness) and nephronophthisis (NPHP, characterized by fibrocystic renal disease) each primarily affect one of three organs frequently diseased in ciliopathies, namely the cerebellum, retina and kidney. These diseases are genetically heterogeneous and are sometimes variable even within single families, undermining the predictive value of diagnostics and genetic counseling. Though many causative genes have been identified for these Mendelian disorders, our current understanding of the underlying genetics and mechanisms is insufficient to explain this variability and suggests the involvement of genetic modifiers.

A likely model for how so many different gene mutations can lead to Joubert syndrome and related diseases is that these protein products physically interact or otherwise cooperate to perform a similar function. In line with this idea is the previously reported finding that AHI1 interacts with nephrocystin-1 (NPHP1)[196], the product of the gene that is the most commonly mutated in juvenile NPHP[66,197].

In humans, mutations in *NPHP1* cause juvenile nephronophthisis with partially penetrant retinopathy. To study *Nphp1* in mouse, we generated a targeted disruption of *Nphp1* by insertion of a neo-bpA cassette into exon 4, which generated a null allele and confirmed absence of Nphp1 expression (Figure 4.1a–c). The photoreceptors of *Nphp1*$^{neo/neo}$ mice (hereafter denoted as *Nphp1*$^{-/-}$) formed outer segments but underwent gradual retinal degeneration, which was slightly evident at 2 months (Figure 4.1d). This was milder than an

independently targeted *Nphp1* mutant reported to show failure of outer segment formation followed by retinal degeneration[198]. Because both *Nphp1* alleles are predicted to function as nulls, this difference in severity of retinal phenotypes suggests the influence of genetic modifiers.

To test whether genetic interaction between *Ahi1* and *Nphp1* can influence phenotypic expression *in vivo*, we examined double- mutant combinations of *Ahi1* and *Nphp1* alleles, ranging from single heterozygotes to knockout-heterozygote combinations, for outer nuclear layer (ONL) thickness and for mislocalized opsin. To efficiently obtain *Ahi1* homozygous null genotypes, we used the $Ahi1^{flox}$ allele and the distal (peripheral) retina-specific Pax6α-Cre transgene[191] to circumvent the lethality associated with $Ahi1^{-/-}$. We observed trends of increasing severity of cell loss and opsin redistribution with additional deleterious alleles with the *Ahi1* null allele showing a stronger effect (Figure 4.2a). Specifically, we found significantly decreased ONL thickness and increased ONL-localized opsin when we compared $Nphp1^{-/-}Ahi1^{+/-}$ against $Nphp1^{-/-}$- and $Ahi1^{+/-}$-only controls at P21 (Figure 4.2b). These data suggest that dosage-sensitive genetic interactions occur between *Ahi1* and *Nphp1* in retinal development.

Based on the pronounced retinopathy in $Ahi1^{-/-}$ mice, we next tested whether *AHI1* was mutated in humans with isolated LCA. In a screen of *AHI1*-coding exons from well-characterized individuals with LCA (from the United States, Canada, The Netherlands and Spain, prescreened for mutations in

known LCA genes; *n* = 176), no homozygous or compound heterozygous deleterious changes were identified (Table 4.1). However, one variant, R830W-C2488T, heterozygous in nine independent cases, was of particular interest, though it was not significantly enriched in affected individuals compared to controls. Arg830 is conserved throughout vertebrate homologs, and in addition, a change from arginine to tryptophan (from a polar basic residue to a nonpolar hydrophobic residue) is predicted to be damaging to AHI1 (Polyphen[199] and SNPs3D[200]). This, coupled with its position within the WD40 repeat domain (between two blades of its predicted propeller structure; Figure 4.3a,b), suggested that this substitution might interfere with the function of AHI1, perhaps in protein-protein interactions.

To test whether this change altered sedimentation of AHI1 complexes *in vitro*, we expressed GFP-AHI1 with the R830W substitution, wild-type GFP-AHI1 or GFP-EV (empty vector) in cells from the HEK293T line with untagged human rhodopsin[201] (RHO) and assayed lysates by sucrose density gradients (Figure 4.3c). We identified two distinct sedimentation peaks containing AHI1 that appeared at lower intensity for GFP-AHI1 R830W–transfected cells; this decrease suggests under-representation of AHI1 R830W in complexes, despite comparable total expression levels of AHI1 R830W and wild-type AHI1 or empty-vector controls in HEK293T cells (Figure 4.3d). Furthermore, opsin was shifted toward lower-density complexes in cells expressing AHI1 R830W compared to those expressing wild-type AHI1 or empty vector. This lends support to

potentially hypomorphic effects of R830W, perhaps in complex stability or formation. This variant has been mentioned as a polymorphism in several *AHI1* studies[1,2,202,203], but the effect of the change on retinal disease has not been explored. Due to the genetic interaction of *Ahi1* and *Nphp1* in mice and the variable association of retinal degeneration with nephronophthisis (also known as Senior-Løken syndrome, SLSN[204]), we hypothesized that *AHI1* R830W might contribute to the risk of retinopathy in nephronophthisis patients.

We thus genotyped 153 independent individuals with nephronophthisis from Italy (of which 16 had retinal degeneration) and 306 ethnically matched healthy controls for the R830W (C2488T) change. We found that the T-allele frequency was significantly higher in individuals with NPHP and retinal degeneration versus those with NPHP excluded for retinal degeneration (25% compared to 1.8%, $P = 5.36 \times 10^{-6}$, (Table 4.2) and versus controls (25% compared to 2.8%, $P = 9.03 \times 10^{-6}$; Table 4.2). This translated to a relative risk of 7.5 (95% CI 4.0–11.2) associated with *AHI1* R830W for retinal degeneration within NPHP patients. To determine if this association depended upon the primary gene mutation, we repeated this analysis after subdividing affected individuals into those with *NPHP1* mutations (either homozygous or compound heterozygous mutation) versus those without *NPHP1* mutations. *AHI1* R830W continued to be significantly associated with NPHP in the presence of retinal degeneration irrespective of the primary mutation (Table 4.2).

To control for population stratification, we also examined transmission of R830W in this cohort[205] by genotyping parents of 117 available trios. We found 17 informative trios where one parent was heterozygous for C2488T. Although this sample size was too limited for full transmission disequilibrium test analysis, we found that the T allele was over-transmitted to individuals with both NPHP and retinal degeneration. Specifically, the T allele was transmitted 100% of the time to individuals with NPHP and retinal degeneration ($n = 7$, $P < 0.01$, χ^2 test) but only 50% of the time to individuals with NPHP without retinal degeneration ($n = 10$, no significant difference from the null hypothesis). This association was apparent when evaluating single families; for example, in one family with three individuals with NPHP[204], *AHI1* R830W segregated only with the sibling showing an absent ERG response, whereas the other siblings retained visual function. Our results support a role for *AHI1* as a modifier of retinal degeneration in the context of mutations leading to NPHP.

That this *AHI1* allele is associated with retinal disease in as many as half of individuals with SLSN in this Italian population suggests that other, rarer *AHI1* variants may behave similarly. Results from the mouse models support a role for Ahi1 in cilia-associated trafficking mechanisms, consistent with the results of a recent study describing Ahi1 function in cultured cells[206]. We also identify a new role for Ahi1 in photoreceptor development and demonstrate the utility of mouse genetic interaction studies in identifying loci conferring high-risk alleles for disease. A similar effect was reported for one variant of *RPGRIP1L*[207], supporting

the role of modifiers in phenotypic expressivity of ciliopathies. Given the complexity of ciliopathy phenotypes, it is likely that other variable phenotypes could also be explained by genetic modifiers. Notably, a cohort of individuals with Joubert syndrome (n = 155) did not reveal a significant difference in frequency of *AHI1*R830W, although R830W was found with slightly higher frequency in affected individuals relative to controls. These individuals were ascertained for having phenotypes associated with a specific constellation of midbrain-hindbrain malformations but also for having variably present renal and/or retinal dysfunction. Lack of significant association with Joubert syndrome may reflect more complex interactions at the molecular level, requiring specific disruptions to alter phenotypic expression. Future screenings at other loci may help elucidate these distinct but overlapping mechanisms. Our example within the ciliopathies shows that mutational analysis of other causative genes from the broader clinical spectrum can yield substantial insight into the genetics and pathogenesis of heterogeneous syndromic disorders.

METHODS

Subjects and mutational screening.

Subjects were ascertained from populations of European ancestry (Italian, French/French Canadian, Spanish and Dutch) based on clinical features specific to LCA, NPHP and Joubert syndrome (with the exception of the NPHP group, which was mostly of Italian ancestry). In particular, NPHP cases were ascertained over 15 years at the Nephrology Center of the G. Gaslini Childrens

Hospital (Genoa, Italy)[37]. Diagnosis of NPHP was based on bioclinical tests, kidney and liver ultrasound, ophthalmologic examination and molecular tests (for *NPHP1* deletion and/or mutations). All affected individuals showed clinical and laboratory signs of NPHP, including urinary concentration defect, increase of serum creatinine levels above the normal range for age and small hyperechoic kidneys without corticomedullary differentiation. More than 70% of cases had already developed end-stage renal failure (ESRF), and most of those with ESRF had received kidney transplants. Affected individuals with possible neurological involvement underwent detailed neurological testing, including brain MRI and EEG. Individuals with Joubert syndrome were ascertained through the International JSRD Study Group, referring cases from several countries worldwide. The clinical diagnosis was confirmed by brain neuroimaging showing the typical 'molar tooth sign'. A standardized clinical questionnaire was obtained to assess extent of multiorgan involvement. Control subjects were drawn from the same populations and represented subjects who were healthy with respect to the clinical signs of interest. Informed consent was obtained for all subjects according to approved institutional human subjects protocols (Human Research Protection Program Committees of UCSD, La Jolla and the CSS-Mendel Institute, Rome).

Exons were PCR-amplified and sequenced using BigDye Terminator chemistry (ABI Prism 3100), and chromatograms were analyzed visually; or PCR fragments were analyzed on a DHPLC-based WAVE DNA Fragment Analysis

System (Transgenomic, Crewe). Samples with abnormal elution profiles underwent direct bidirectional sequencing as above. Primer sequences were published previously[1].

Generation of Nphp1 *mutant mice.*

To clone the mouse *Nphp1* locus, a 129/Ola genomic cosmid library (obtained from the Resourcenzentrum Berlin) was probed using the mouse cDNA. A single cosmid clone was purified, and a 10-kb SacI and 12-kb EcoRI fragment harboring the exon 4 region of the *Nphp1* transcription unit were subcloned and characterized by restriction mapping. To generate a targeting construct for *Nphp1*, a 12.5-kb genomic fragment derived from the two subfragments was modified by inserting a floxed PGK-neobpA cassette (*pMC1-neo-polyA*) into a unique NheI site. The targeting vector was linearized at a unique SalI site and introduced into cells of the E14 ES cell line[208]. 159 G418-resistant colonies were screened by DNA blot analysis and four correctly targeted ES cell lines were identified. *Nphp1*$^{neo/+}$ ES cells (129/Ola) were microinjected into NMRI albino mouse blastocysts to generate chimeras. Males with high degree of chimerism were mated to NMRI females for germline transmission. F1 heterozygous males were crossed to NMRI females and heterozygous offspring were intercrossed. Mice were genotyped by DNA blotting using a BamHI RFLP with the floxed neo-cassette (wild-type allele, 40 kb; mutant, 20 kb), or by PCR, with primers amplifying a 120-bp fragment (wild type) and a 1,600-bp fragment (mutant) (Table, add or omit)

Antibodies and fluorescence microscopy.

Mice were anesthetized by isoflurane inhalation and perfused, or eyes were immersed in 4% paraformaldehyde/PBS. 10–25-μm cryosections corresponding to a medial position (intersecting optic nerve) were stained for immunofluorescence per standard protocols except where noted. We used the primary antibody mouse anti-opsin (1:250, Chemicon). We used Alexa Fluor dye-conjugated secondary antibodies (1:750, Invitrogen/Molecular Probes) and Hoechst 33342 (1:10,000) nuclear dye. Images were obtained on a Fluoview1000 Spectral Deconvolution Confocal microscope (Olympus), under the same parameters for each experiment.

Opsin immunofluorescence measurements were determined from raw images using NIH ImageJ software ('Measure RBG' plug-in). ONL values were normalized to values from the apical region encompassing IS and OS. Measurements were made on comparable regions of the retina (minimum two per section, from central and peripheral regions and averaged together, with the exception of Pax6α-Cre cKOs, for which all measurements were from peripheral (distal) regions).

Cell culture and transfection.

HEK293T (human embryonic kidney) cells were seeded on 10-cm culture plates at 40% density by surface area and transfected the following day at 90%–95% confluency by Lipofectamine 2000 (Invitrogen) using 24 μg total DNA per plate. Cells were lysed 24 h later for analysis.

Protein blotting and sucrose fractionation.

Protein blotting was performed on lysates prepared in modified RIPA buffer using the following antibodies: rabbit anti-Ahi1, mouse anti-GFP (Covance, B34), mouse anti–α-tubulin (Sigma, T-6074) and mouse anti-rhodopsin (Chemicon, MAB5316). All antibodies were diluted 1:1,000 in 4% milk. Secondary detection was performed using horseradish peroxidase–conjugated anti-mouse or anti-rabbit antibodies (1:20,000, Zymax) in 4% milk. For sucrose fractionation, modified RIPA lysates were loaded onto stepwise gradients from 5%–60% sucrose followed by ultracentrifugation overnight at 100,000*g* force. Fractions were collected from the top, and protein was precipitated using trichloroacetic acid followed by SDS-PAGE and protein blotting.

Statistics.

For the association studies, two-tailed *P* values were computed using Fisher's exact test using the sum-of-small-*P*-values method (see URL section). The TDT (χ^2) statistic[205] was computed manually with *P* value assigned for 1 degree of freedom. Relative risk and confidence intervals were computed (see URL section) based on a general method[209]. For other studies, data were expressed as means ± s.e.m. Two-tailed *P* values were calculated by Student's *t*-test. Values <0.05 were considered statistically significant for all tests.

URLs.

Fisher's exact test, http://www.langsrud.com/fisher.htm; risk and confidence intervals, http://statpages.org/ctab2x2.html.

ACKNOWLEDGEMENTS

Work in Chapter 4 was published as: Louie, Carrie M; Caridi, Gianluca; Lopes, Vanda S; Brancati, Francesco; Kispert, Andreas; Lancaster, Madeline A; Schlossman, Andrew M; Otto, Edgar A; Leitges, Michael; Hermann-Josef Gröne; Lopez, Irma; Gudiseva, Harini V; O'Toole, John F; Vallespin, Elena; Ayyagari, Radha; Ayuso, Carmen; Cremers, Frans PM; I den Hollander, Anneke; Koenekoop, Robert K; Dallapiccola, Bruno; Ghiggeri, Gian Marco; Hildebrandt, Friedhelm; Valente, Enza Maria; Williams, David S; Gleeson, Joseph G. *AHI1* is required for photoreceptor outer segment development and is a modifier for retinal degeneration in nephronophthisis. *Nature Genetics* vol. 42, p175-180 (2010); advance online publication, 17 Jan 2010 (doi:10.1038/ng.519). The dissertation author was the primary investigator and author of this paper.

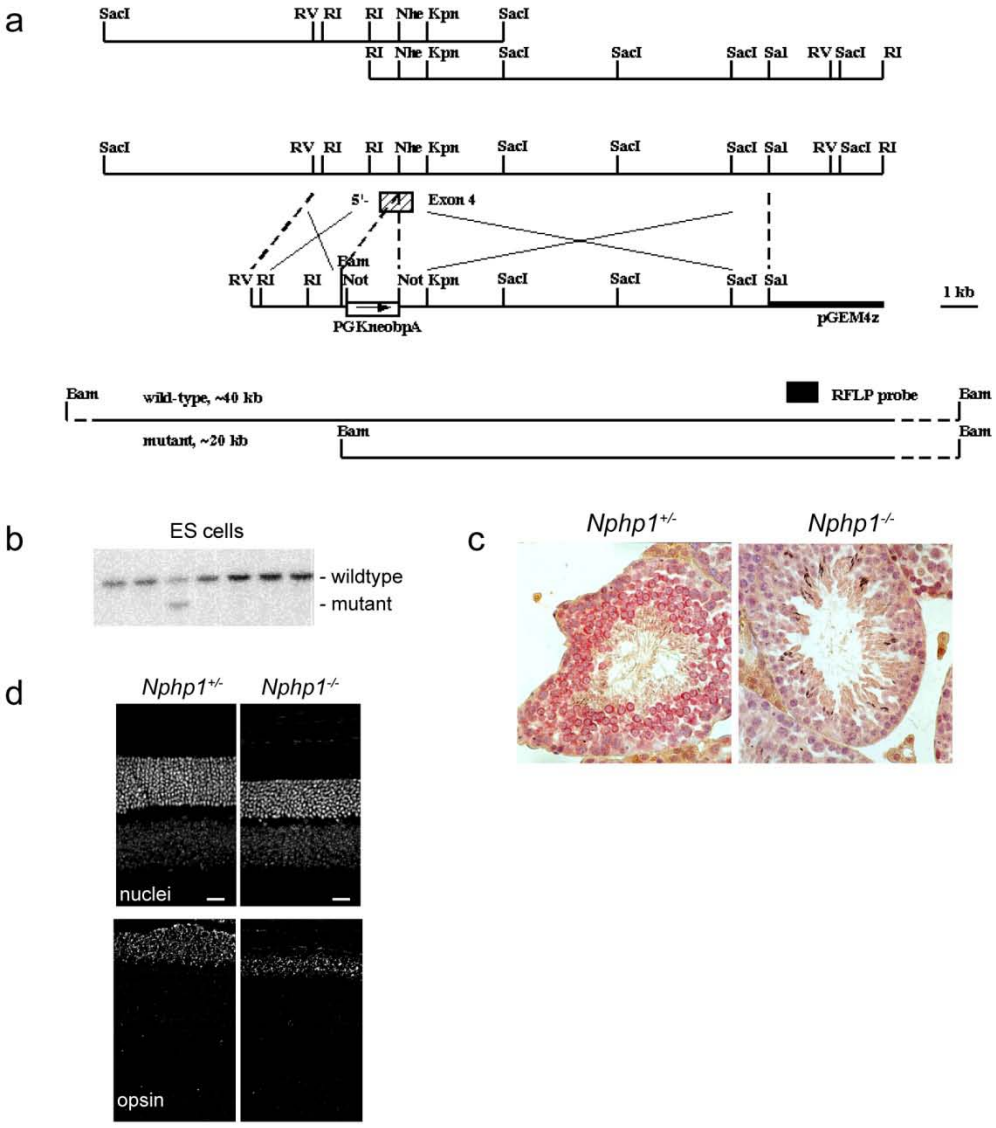

Figure 4.1 *Nphp1* mouse targeting and mild retinal phenotype **(a)** Restriction map of the murine *Nphp1* locus and targeting construct. The *Nphp1* gene was disrupted in exon 4 by a PGK-neobpA cassette **(b)** RFLP probe on Southern blot detected 20 kb truncated BamHI fragment in the mutant relative to the wildtype 40 kb fragment **(c)** Nphp1 (red) in testis from *Nphp1*$^{+/-}$ and *Nphp1*$^{-/-}$ confirming absence of Nphp1 in the knockout **(d)** *Nphp1*$^{+/+}$ and *Nphp1*$^{-/-}$ retina at 8 wks stained for rhodopsin (green) and nuclei (Hoescht 33342, blue). Scale=20μm

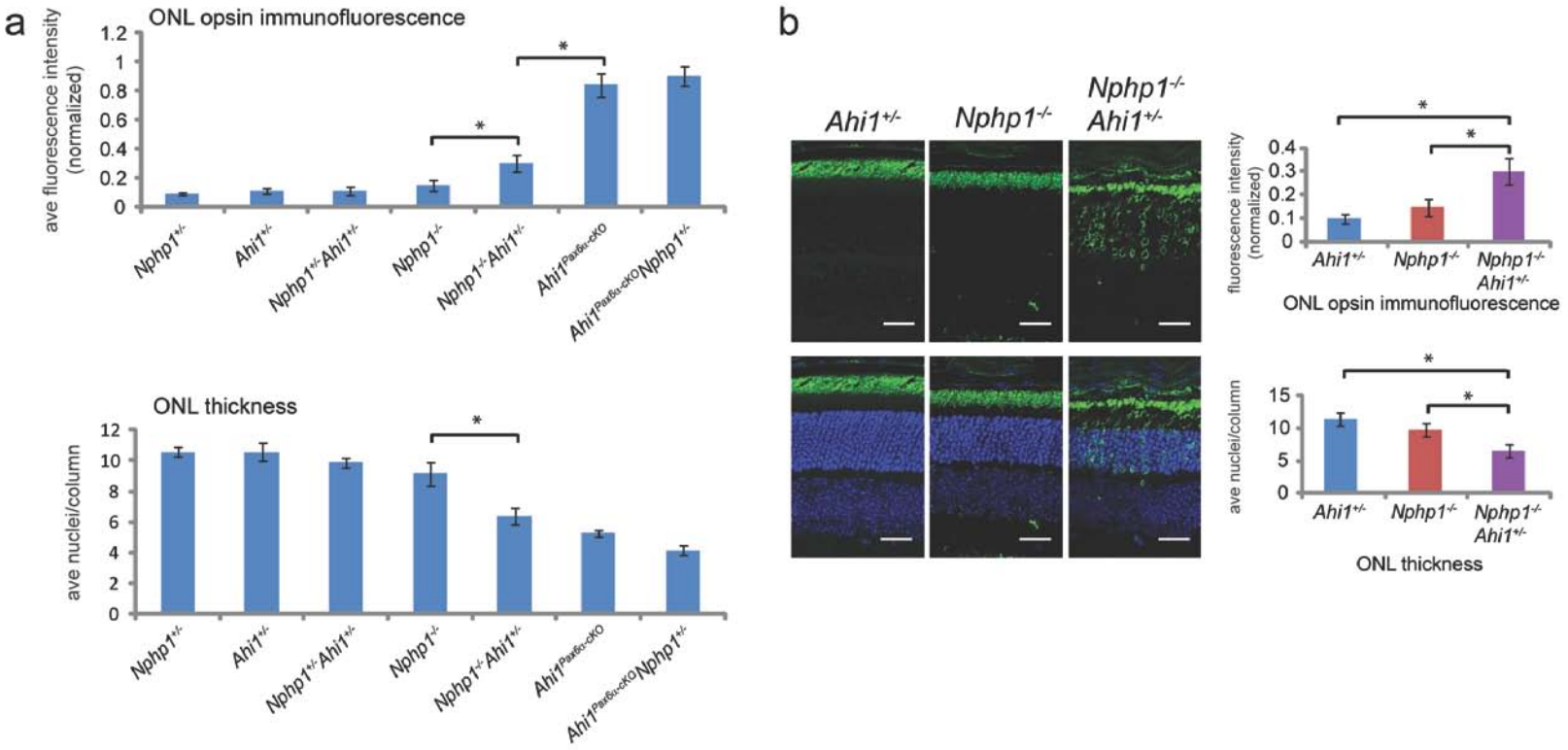

Figure 4.2 Genetic interaction of *Ahi1* with *Nphp1*. **(a)** Increased cell loss and redistribution of opsin with increased load of deleterious *Ahi1* and *Nphp1* alleles in mouse retina. Quantification of opsin immunofluorescence (green) from ONL (outer nuclear layer, normalized as fluorescence ratio of ONL/apical region encompassing inner (IS) and outer (OS) segments), and quantification of outer nuclear layer (ONL) thickness, expressed as averaged number of nuclei per column (indicated by Hoechst 33342 staining) from 10-µm cryosections from indicated genotypes at P21. **(b)** As indicated in a, the *Ahi1*-null allele modifies the $Nphp1^{-/-}$ phenotype, with $Nphp1^{-/-}Ahi1^{+/-}$ showing increased opsin accumulation and decreased thickness of the ONL versus $Nphp1^{-/-}$ and $Ahi1^{+/-}$ controls. Asterisk denotes significant difference from both $Ahi1^{+/-}$ and $Nphp1^{-/-}$; n = 6–7, $P_{\text{ONL thickness}}$ = 0.00315 and 0.000106, respectively; $P_{\text{fluorescence}}$ = 0.0454 and 0.0141, respectively. Scale bar, 20 µm. Error bars, s.e.m.

Table 4.1 *AHI1* variants identified from screen of 176 LCA patients

Subject ID	amino acid change	Ethnicity	Other mutations known	SNP ID
006/966	S1123F	Spain		
KE465	G762A	American		
KE465	fs753X	American		
03/0908	R830W	Spain		rs13312995
236	R830W	French-Canadian		rs13312995
3364	R830W	French-Canadian		rs13312995
KE556	Q1018P	American		rs6940875
R805	R548H	American		rs35433555
03/1033	R548H	Spain		rs35433555
54	R548H	French-Canadian		rs35433555
3361	L224V	French-Canadian		
490	R835K	French-Canadian		
13888	A607E	Dutch	RPGRIP1L splice mutation	
20898	R830W	Dutch	LCA5 R301H	
27226	R830W	French-Canadian		
27228	R830W	French-Canadian	CEP290p.Cys998X homozygous	
27245	R830W	French-Canadian	CEP290p.Cys998X, p.Ile1372LysfsX4	
27253	R830W	Middle Eastern		
27255	R830W	American		

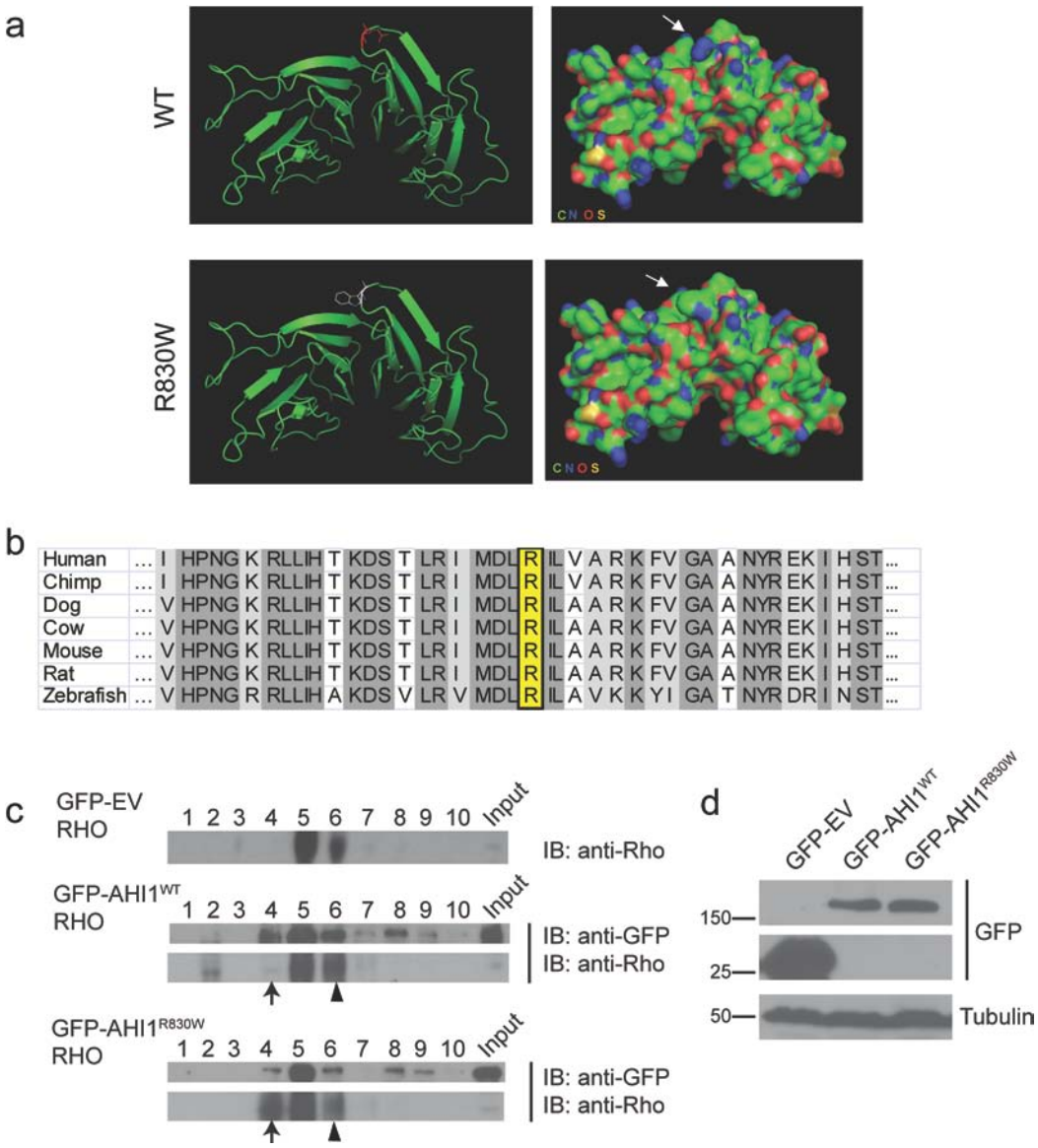

Figure 4.3 *AHI1* p.R830W is a potentially hypomorphic allele of *AHI1* **(a)** Predicted structure (line and surface views) of a portion of the WD40 domain of AHI1 as compiled by PyMOL software (Delano Scientific LLC, educational version). R830W (arrows) is positioned in between two blades of the predicted propeller structure of the WD40 domain **(b)** *AHI1* and homologous sequences showing conservation of R830W throughout vertebrate homologs. Conserved residues shown in gray, with R830W specifically in yellow. **(c)** sucrose density gradient fractionation of cell lysates from HEK293T co-transfected with GFP-AHI1^{R830W} , GFP-AHI1^{WT} or GFP-EV (empty vector) with rhodopsin (RHO), showing shift in rhodopsin containing fraction only when co-transfected with GFP-AHI1^{R830W}. Arrows and arrowheads indicating differences observed in fractions 4 and 6 **(d)** Representative Western blot for AHI1 from HEK293T cells expressing GFP-AHI1^{R830W}, GFP-AHI1^{WT}, and GFP-EV, showing comparable expression levels.

Table 4.2 Frequency of *AHI1* R830W (C2488T) in Italians with nephronophthisis with or without additional retinal

Groups[a]	2*n*	*n*	Genotypes CC	CT	TT	Genotype frequency f(CC)	f(CT)	f(TT)	Alleles C	T	Allele frequency f(C)	f(T)	*P* vs. total controls[b]	*P* RD vs. non-RD
Total controls	612	306	289	17	0	0.944	0.056	0	595	17	0.927	0.028		
NPHP	274	137	132	5	0	0.964	0.036	0	269	5	0.982	**0.018**	ns	
NPHP + RD	32	16	8	8	0	0.500	0.500	0	24	8	0.750	**0.250**	**9.03×10^{-6}**	**5.36×10^{-6}**
Total NPHP	306	153	140	13	0	0.915	0.085	0	293	13	0.958	0.042	ns	
NPHP1	74	37	37	0	0	1.000	0.000	0	74	0	1.000	0.000	ns	
NPHP1 + RD	10	5	2	3	0	0.400	0.600	0	7	3	0.700	0.300	0.0029	0.0013
Total *NPHP1*	84	42	39	3	0	0.929	0.071	0	81	3	0.964	0.036	ns	
Non-*NPHP1*	200	100	95	5	0	0.950	0.050	0	195	5	0.975	0.025	ns	
Non-*NPHP1* + RD	22	11	6	5	0	0.545	0.455	0	17	5	0.773	0.227	0.00056	0.0011
Total non-*NPHP1*	222	111	101	10	0	0.910	0.090	0	212	10	0.955	0.045	ns	

[a]*NPHP1* refers to individuals with NPHP with mutations in the *NPHP1* gene; non-*NPHP1* refers to individuals with NPHP in whom mutations in *NPHP1* have been excluded. [b]Two-tailed *P* values >0.05 were considered not significant (ns). RD, retinal degeneration.

CHAPTER 5: SUMMARY/DISCUSSION

SUMMARY

The motivation of this study was to understand the etiology of Joubert syndrome, a neurodevelopmental syndrome that affects the cerebellum, for which the genetic and molecular basis was not well known. At the time, multiple loci had been mapped and mutations in two genes, AHI1 and NPHP1 were identified to cause a subset of Joubert cases. Interestingly, NPHP1 and several others were known to be involved in a seemingly distinct cystic kidney disease, nephronophthisis, for which the encoded proteins all localized to the primary cilium. This connection led to a ciliary hypothesis for the basis of Joubert syndrome, and was supported by evidence of cilia on neurons throughout the brain, though nothing was known about the function of these organelles. To evaluate this hypothesis and to uncover the mechanisms underlying this disease, I focused on the characterization of the *AHI1* gene.

AHI1 is a WD40 and SH3 domain-containing protein that has been associated with oncogenesis in specific forms of cancer, but its direct function was not known. I and others have shown that AHI1 localizes to the base of the primary cilium using immunochemical and transgenic overexpression techniques. Then, to model the loss of AHI1 *in vivo*, I generated a conditional knockout mouse line for AHI1. Complete null mutants (*Ahi1-/-*) were severely runted at postnatal timepoints and showed high mortality rates, but relatively normal brain

morphology. Consistent with this, mutants did not show signs of ataxia or loss of muscle tone. Knockout cells also did not show evidence of proliferation defects indicated by in vitro studies demonstrating its oncogenic potential. Axon tracing did not reveal an absence of CST decussation that has been reported in human patients. Furthermore, ciliogenesis in the Ahi1-/- appeared to be intact, as shown by the presence of cilia on neurons throughout the cerebellum and other areas of the brain.

Despite these seemingly disparate results, it was becoming clearer that Joubert syndrome was indeed a “ciliopathy” *i.e.*, a genetic disorder of the cilium, as more causative overlapping genes were discovered and more direct roles in ciliary transport (or intraflagellar transport, IFT) were described for related diseases.

Phenotypically, the Joubert spectrum shared many features with other ciliopathies. AHI1 mutations, in particular, are associated with a high incidence of retinopathy in Joubert patients. I examined *Ahi1* null retina and found a rapid degeneration of the photoreceptor cells, consistent with human cases. In photoreceptors, Ahi1 is also localized to the base of the cilium. This structure is uniquely specialized to facilitate visual transduction by providing a large, compartmentalized membranous surface area (as stacked disks—outer segments). In the absence of Ahi1 in mice, these outer segments fail to develop and opsin, its major constituent is redistributed abnormally, leading to apoptotic cell death.

I also found that *Ahi1* alleles could modify the phenotype of another ciliopathy mutant, *Nphp1-/-* mice. These mice have a milder degeneration of the retina and the introduction of a null copy of *Ahi1* significantly worsens this phenotype. In collaboration with several other labs, we found a similar phenomenon in a cohort of Italians with nephronophthisis with or without retinal degeneration, in that a specific variant of *AHI1* was associated with increased risk for retinal degeneration.

DISCUSSION

Several possible explanations exist for the discrepancy between mouse and human phenotypes. Although AHI1 is fairly conserved between human and mouse, it is possible that these orthologs do not share precisely the same function. The N-terminal regions (containing the NLS sequences and coiled-coil domain) between these two sequences show a greater divergence from one another compared to the rest of gene (containing the WD40 repeats and SH3 domain). For WD40 repeat proteins, which are known to have diverse functions, this could have resulted in distinct specializations of AHI1 function or regulation. Consistent with this, a previous report that human *AHI1* exhibits a higher rate of nonsynonymous substitution compared to other lineages, suggests that human *AHI1* has undergone stronger selective pressure[126]. The authors of this study go on to propose that this selection may have been driven by a specialization of *AHI1* towards higher cognitive functions in the human brain. The association of

the AHI1 locus with schizophrenia and autism could reflect such a function, while simultaneously explaining the relatively mild brain phenotype of *Ahi1-/-* mice.

Another plausible explanation is that the effects of these ciliopathy mutations are strongly influenced by genetic background. This could be due to inherent differences between mouse and human genomes or this could be due to the specific modifying alleles present in a heterogenous human population versus the inbred mouse line. The evidence for genetic interaction between Ahi1 and Nphp1 in mouse presented in this study support the idea that differences in the mouse and human phenotypes may be due to modifier effects. Such effects have been better described in human ciliopathy studies, especially in the case of Bardet Biedl syndrome and more recently with the RPGRIP1L modifying variant. The model of “triallelic” inheritance proposed for BBS may very well be prevalent throughout the broad spectrum of ciliopathies. In the mouse, it may be possible to discover similar genetic relationships by studying combinations of mutations that lead to more precise models of ciliopathies.

Overall, these results show that Ahi1 is required for the development of photoreceptor outer segments, most likely in facilitating ciliary trafficking. The photoreceptor degeneration appears to be due to a toxic accumulation of opsin that is secondary to this outer segment defect.

These findings also highlight the complexity of heterogeneous syndromic disease and suggest that perturbation of more than gene may be involved in the pathogenesis even of these Mendelian disorders. Despite the differences

between human and mouse with respect to penetrance of brain phenotypes, I have found that the *Ahi1* knockout mouse remains an informative and relevant model for ciliopathies.

FUTURE DIRECTIONS AND MODEL

Many questions remain in the study of cilia in neurodevelopmental disease. For this study in particular, it remains to be shown what the precise relationship is between AHI1 and outer segment development—is AHI1 directly needed for the trafficking of opsin? What is the role of AHI1 in other tissues and how might this be leading to the runting and survival problems seen in the *Ahi1-/-* mouse?

With regards to the retina, this study suggests a model for Ahi1 function that reflects the importance of photoreceptor ciliary trafficking, possibly in the loading or sorting of cargo at the base/transition zone of the photoreceptor cilium. This is likely regulated in concert with other Joubert proteins such as Nphp1, and also likely with those of other disorders such as the “BBsome” associated with Bardet Biedl syndrome. Current evidence is pointing to a specific role for the BBSome in vesicular sorting to the cilium[210], but the precise function of Ahi1 and other Joubert-associated proteins remain unclear.

In terms of the other questions, it would be relevant to examine whether the runting/early lethality is due to a problem of feeding behavior which has been shown to be affected in mutants with defective cilia (in the hypothalamus).

Another intriguing future study would be to determine whether a cilia mutant such as the *Ahi1-/-* could model schizophrenia as implied by human association studies.

With the increasing accessibility of genetic screening technologies, new causative genes are rapidly being identified. This will be necessary for learning the full scope of the mechanisms and the players involved in the pathogenesis of Joubert syndrome and related diseases. Equally, if not more importantly, the direct mechanisms by which AHI1 and other Joubert proteins function at the cellular level remains to be shown definitively. Although BBS proteins seem to cooperate as a complex (the BBSome), whether a similar “JBTSome” exists is less obvious, and a common function for Joubert proteins has yet to be defined. Whatever this may be, it is clear that it will be necessary to consider these genes/proteins in the context of the broader group of cilia genes/proteins in order to understand how their disruption could lead to disease.

REFERENCES

1. Valente, E.M. et al. AHI1 gene mutations cause specific forms of Joubert syndrome-related disorders. *Ann Neurol* **59**, 527-34 (2006).

2. Parisi, M.A. et al. AHI1 mutations cause both retinal dystrophy and renal cystic disease in Joubert syndrome. *J Med Genet* **43**, 334-9 (2006).

3. Badano, J.L., Mitsuma, N., Beales, P.L. & Katsanis, N. The ciliopathies: an emerging class of human genetic disorders. *Annu Rev Genomics Hum Genet* **7**, 125-48 (2006).

4. Quinlan, R.J., Tobin, J.L. & Beales, P.L. Modeling ciliopathies: Primary cilia in development and disease. *Curr Top Dev Biol* **84**, 249-310 (2008).

5. Kozminski, K.G., Johnson, K.A., Forscher, P. & Rosenbaum, J.L. A motility in the eukaryotic flagellum unrelated to flagellar beating. *Proc Natl Acad Sci U S A* **90**, 5519-5523 (1993).

6. Kozminski, K.G., Beech, P.L. & Rosenbaum, J.L. The Chlamydomonas kinesin-like protein FLA10 is involved in motility associated with the flagellar membrane. *J Cell Biol* **131**, 1517-1527 (1995).

7. Cole, D.G. et al. Chlamydomonas kinesin-II-dependent intraflagellar transport (IFT): IFT particles contain proteins required for ciliary assembly in Caenorhabditis elegans sensory neurons. *J Cell Biol* **141**, 993-1008 (1998).

8. Pazour, G.J., Wilkerson, C.G. & Witman, G.B. A dynein light chain is essential for the retrograde particle movement of intraflagellar transport (IFT). *J Cell Biol* **141**, 979-92 (1998).

9. Li, J.B. et al. Comparative genomics identifies a flagellar and basal body proteome that includes the BBS5 human disease gene. *Cell* **117**, 541-552 (2004).

10. Avidor-Reiss, T. et al. Decoding cilia function: defining specialized genes required for compartmentalized cilia biogenesis. *Cell* **117**, 527-39 (2004).

11. Liu, Q. et al. The proteome of the mouse photoreceptor sensory cilium complex. *Mol Cell Proteomics* **6**, 1299-317 (2007).

12. Inglis, P.N., Boroevich, K.A. & Leroux, M.R. Piecing together a ciliome. *Trends Genet* **22**, 491-500 (2006).

13. Huangfu, D. et al. Hedgehog signalling in the mouse requires intraflagellar transport proteins. *Nature* **426**, 83-87 (2003).

14. Liu, A., Wang, B. & Niswander, L.A. Mouse intraflagellar transport proteins regulate both the activator and repressor functions of Gli transcription factors. *Development* **132**, 3103-3111 (2005).

15. Corbit, K.C. et al. Vertebrate Smoothened functions at the primary cilium. *Nature* **437**, 1018-21 (2005).

16. May, S.R. et al. Loss of the retrograde motor for IFT disrupts localization of Smo to cilia and prevents the expression of both activator and repressor functions of Gli. *Dev Biol* **287**, 378-89 (2005).

17. Haycraft, C.J. et al. Gli2 and Gli3 localize to cilia and require the intraflagellar transport protein polaris for processing and function. *PLoS Genet* **1**, e53 (2005).

18. Maria, B.L. et al. "Joubert syndrome" revisited: key ocular motor signs with magnetic resonance imaging correlation. *J Child Neurol* **12**, 423-430 (1997).

19. Joubert, M., Eisenring, J.J., Robb, J.P. & Andermann, F. Familial agenesis of the cerebellar vermis. A syndrome of episodic hyperpnea, abnormal eye movements, ataxia, and retardation. *Neurology* **19**, 813-825 (1969).

20. Boltshauser, E. & Isler, W. Joubert syndrome: episodic hyperpnea, abnormal eye movements, retardation and ataxia, associated with dysplasia of the cerebellar vermis. *Neuropadiatrie* **8**, 57-66 (1977).

21. Maria, B.L., Boltshauser, E., Palmer, S.C. & Tran, T.X. Clinical features and revised diagnostic criteria in Joubert syndrome. *J Child Neurol* **14**, 583-590; discussion 590-591 (1999).

22. Holroyd, S., Reiss, A.L. & Bryan, R.N. Autistic features in Joubert syndrome: a genetic disorder with agenesis of the cerebellar vermis. *Biol Psychiatry* **29**, 287-294 (1991).

23. Ozonoff, S., Williams, B.J., Gale, S. & Miller, J.N. Autism and autistic behavior in Joubert syndrome. *J Child Neurol* **14**, 636-641 (1999).

24. Gleeson, J.G. et al. Molar tooth sign of the midbrain-hindbrain junction: occurrence in multiple distinct syndromes. *Am J Med Genet A* **125**, 125-134; discussion 117 (2004).

25. Gentile, M. et al. COACH syndrome: report of two brothers with congenital hepatic fibrosis, cerebellar vermis hypoplasia, oligophrenia, ataxia, and mental retardation. *Am J Med Genet* **64**, 514-520 (1996).

26. Verloes, A. & Lambotte, C. Further delineation of a syndrome of cerebellar vermis hypo/aplasia, oligophrenia, congenital ataxia, coloboma, and hepatic fibrosis. *Am J Med Genet* **32**, 227-232 (1989).

27. Al-Gazali, L.I., Sztriha, L., Punnose, J., Shather, W. & Nork, M. Absent pituitary gland and hypoplasia of the cerebellar vermis associated with partial ophthalmoplegia and postaxial polydactyly: a variant of orofaciodigital syndrome VI or a new syndrome? *J Med Genet* **36**, 161-166 (1999).

28. Satran, D., Pierpont, M.E. & Dobyns, W.B. Cerebello-oculo-renal syndromes including Arima, Senior-Loken and COACH syndromes: more than just variants of Joubert syndrome. *Am J Med Genet* **86**, 459-469 (1999).

29. King, M.D., Dudgeon, J. & Stephenson, J.B. Joubert's syndrome with retinal dysplasia: neonatal tachypnoea as the clue to a genetic brain-eye malformation. *Arch Dis Child* **59**, 709-718 (1984).

30. Ivarsson, S.A. et al. Joubert syndrome associated with Leber amaurosis and multicystic kidneys. *Am J Med Genet* **45**, 542-547 (1993).

31. Lewis, S.M. et al. Joubert syndrome with congenital hepatic fibrosis: an entity in the spectrum of oculo-encephalo-hepato-renal disorders. *Am J Med Genet* **52**, 419-426 (1994).

32. Egger, J., Bellman, M.H., Ross, E.M. & Baraitser, M. Joubert-Boltshauser syndrome with polydactyly in siblings. *J Neurol Neurosurg Psychiatry* **45**, 737-739 (1982).

33. Houdou, S., Ohno, K., Takashima, S. & Takeshita, K. Joubert syndrome associated with unilateral ptosis and Leber congenital amaurosis. *Pediatr Neurol* **2**, 102-105 (1986).

34. Kher, A.S., Chattopadhyay, A., Divekar, A., Khambekar, K. & Bharucha, B.A. Joubert syndrome with polydactyly and optic coloboma in two sibs. *Indian J Pediatr* **61**, 729-732 (1994).

35. Parisi, M.A. et al. The NPHP1 gene deletion associated with juvenile nephronophthisis is present in a subset of individuals with Joubert syndrome. *Am J Hum Genet* **75**, 82-91 (2004).

36. Castori, M. et al. NPHP1 gene deletion is a rare cause of Joubert syndrome related disorders. *J Med Genet* **42**, e9 (2005).

37. Martinez, S. & Alvarado-Mallart, R.M. Rostral Cerebellum Originates from the Caudal Portion of the So-Called 'Mesencephalic' Vesicle: A Study Using Chick/Quail Chimeras. *Eur J Neurosci* **1**, 549-560 (1989).

38. Hallonet, M.E., Teillet, M.A. & Le Douarin, N.M. A new approach to the development of the cerebellum provided by the quail-chick marker system. *Development* **108**, 19-31 (1990).

39. Martinez, S., Wassef, M. & Alvarado-Mallart, R.M. Induction of a mesencephalic phenotype in the 2-day-old chick prosencephalon is preceded by the early expression of the homeobox gene en. *Neuron* **6**, 971-981 (1991).

40. Heikinheimo, M., Lawshe, A., Shackleford, G.M., Wilson, D.B. & MacArthur, C.A. Fgf-8 expression in the post-gastrulation mouse suggests roles in the development of the face, limbs and central nervous system. *Mech Dev* **48**, 129-138 (1994).

41. Crossley, P.H., Martinez, S. & Martin, G.R. Midbrain development induced by FGF8 in the chick embryo. *Nature* **380**, 66-68 (1996).

42. Wilkinson, D.G., Bailes, J.A. & McMahon, A.P. Expression of the proto-oncogene int-1 is restricted to specific neural cells in the developing mouse embryo. *Cell* **50**, 79-88 (1987).

43. Davis, C.A., Noble-Topham, S.E., Rossant, J. & Joyner, A.L. Expression of the homeo box-containing gene En-2 delineates a specific region of the developing mouse brain. *Genes Dev* **2**, 361-371 (1988).

44. Gardner, C.A., Darnell, D.K., Poole, S.J., Ordahl, C.P. & Barald, K.F. Expression of an engrailed-like gene during development of the early embryonic chick nervous system. *J Neurosci Res* **21**, 426-437 (1988).

45. Asano, M. & Gruss, P. Pax-5 is expressed at the midbrain-hindbrain boundary during mouse development. *Mech Dev* **39**, 29-39 (1992).

46. Rowitch, D.H. & McMahon, A.P. Pax-2 expression in the murine neural plate precedes and encompasses the expression domains of Wnt-1 and En-1. *Mech Dev* **52**, 3-8 (1995).

47. Liu, A. & Joyner, A.L. Early anterior/posterior patterning of the midbrain and cerebellum. *Annu Rev Neurosci* **24**, 869-896 (2001).

48. Pierce, E.T. Histogenesis of the deep cerebellar nuclei in the mouse: an autoradiographic study. *Brain Res* **95**, 503-518 (1975).

49. Altman, J. & Bayer, S.A. Prenatal development of the cerebellar system in the rat. I. Cytogenesis and histogenesis of the deep nuclei and the cortex of the cerebellum. *J Comp Neurol* **179**, 23-48 (1978).

50. Wingate, R.J. & Hatten, M.E. The role of the rhombic lip in avian cerebellum development. *Development* **126**, 4395-4404 (1999).

51. Dahmane, N. & Ruiz-i-Altaba, A. Sonic hedgehog regulates the growth and patterning of the cerebellum. *Development* **126**, 3089-3100 (1999).

52. Wechsler-Reya, R.J. & Scott, M.P. Control of neuronal precursor proliferation in the cerebellum by Sonic Hedgehog. *Neuron* **22**, 103-114 (1999).

53. Ben-Arie, N. et al. Evolutionary conservation of sequence and expression of the bHLH protein Atonal suggests a conserved role in neurogenesis. *Hum Mol Genet* **5**, 1207-1216 (1996).

54. Yang, X.W., Zhong, R. & Heintz, N. Granule cell specification in the developing mouse brain as defined by expression of the zinc finger transcription factor RU49. *Development* **122**, 555-566 (1996).

55. Alder, J., Cho, N.K. & Hatten, M.E. Embryonic precursor cells from the rhombic lip are specified to a cerebellar granule neuron identity. *Neuron* **17**, 389-399 (1996).

56. Aruga, J. et al. A novel zinc finger protein, zic, is involved in neurogenesis, especially in the cell lineage of cerebellar granule cells. *J Neurochem* **63**, 1880-1890 (1994).

57. Hatten, M.E. & Heintz, N. Mechanisms of neural patterning and specification in the developing cerebellum. *Annu Rev Neurosci* **18**, 385-408 (1995).

58. Wang, V.Y. & Zoghbi, H.Y. Genetic regulation of cerebellar development. *Nat Rev Neurosci* **2**, 484-491 (2001).

59. Yachnis, A.T. & Rorke, L.B. Neuropathology of Joubert syndrome. *J Child Neurol* **14**, 655-659; discussion 669-672 (1999).

60. Martin, J.H. The corticospinal system: from development to motor control. *Neuroscientist* **11**, 161-173 (2005).

61. ten Donkelaar, H.J., Hoevenaars, F. & Wesseling, P. A case of Joubert's syndrome with extensive cerebral malformations. *Clin Neuropathol* **19**, 85-93 (2000).

62. Parisi, M.A. et al. Cerebral and cerebellar motor activation abnormalities in a subject with Joubert syndrome: functional magnetic resonance imaging (MRI) study. *J Child Neurol* **19**, 214-218 (2004).

63. Saunier, S., Salomon, R. & Antignac, C. Nephronophthisis. *Curr Opin Genet Dev* **15**, 324-331 (2005).

64. Hildebrandt, F., Attanasio, M. & Otto, E. Nephronophthisis: disease mechanisms of a ciliopathy. *J Am Soc Nephrol* **20**, 23-35 (2009).

65. Otto, E.A. et al. Hypomorphic mutations in meckelin (MKS3/TMEM67) cause nephronophthisis with liver fibrosis (NPHP11). *J Med Genet* **46**, 663-70 (2009).

66. Hildebrandt, F. et al. A novel gene encoding an SH3 domain protein is mutated in nephronophthisis type 1. *Nat Genet* **17**, 149-153 (1997).

67. Otto, E.A. et al. Mutations in INVS encoding inversin cause nephronophthisis type 2, linking renal cystic disease to the function of primary cilia and left-right axis determination. *Nat Genet* **34**, 413-420 (2003).

68. Olbrich, H. et al. Mutations in a novel gene, NPHP3, cause adolescent nephronophthisis, tapeto-retinal degeneration and hepatic fibrosis. *Nat Genet* **34**, 455-459 (2003).

69. Mollet, G. et al. The gene mutated in juvenile nephronophthisis type 4 encodes a novel protein that interacts with nephrocystin. *Nat Genet* **32**, 300-305 (2002).

70. Otto, E.A. et al. Nephrocystin-5, a ciliary IQ domain protein, is mutated in Senior-Loken syndrome and interacts with RPGR and calmodulin. *Nat Genet* **37**, 282-288 (2005).

71. Sayer, J.A. et al. The centrosomal protein nephrocystin-6 is mutated in Joubert syndrome and activates transcription factor ATF4. *Nat Genet* **38**, 674-81 (2006).

72. Valente, E.M. et al. Mutations in CEP290, which encodes a centrosomal protein, cause pleiotropic forms of Joubert syndrome. *Nat Genet* **38**, 623-5 (2006).

73. Attanasio, M. et al. Loss of GLIS2 causes nephronophthisis in humans and mice by increased apoptosis and fibrosis. *Nat Genet* **39**, 1018-24 (2007).

74. Wolf, M.T. et al. Mutational analysis of the RPGRIP1L gene in patients with Joubert syndrome and nephronophthisis. *Kidney Int* **72**, 1520-6 (2007).

75. Otto, E.A. et al. NEK8 mutations affect ciliary and centrosomal localization and may cause nephronophthisis. *J Am Soc Nephrol* **19**, 587-92 (2008).

76. Takano, K. et al. Cerebellar and brainstem involvement in familial juvenile nephronophthisis type I. *Pediatr Neurol* **28**, 142-144 (2003).

77. Mollet, G. et al. Characterization of the nephrocystin/nephrocystin-4 complex and subcellular localization of nephrocystin-4 to primary cilia and centrosomes. *Hum Mol Genet* **14**, 645-656 (2005).

78. Morgan, D. et al. Inversin, a novel gene in the vertebrate left-right axis pathway, is partially deleted in the inv mouse. *Nat Genet* **20**, 149-156 (1998).

79. Ibanez-Tallon, I., Heintz, N. & Omran, H. To beat or not to beat: roles of cilia in development and disease. *Hum Mol Genet* **12 Spec No 1**, R27-35 (2003).

80. Okada, Y. et al. Abnormal nodal flow precedes situs inversus in iv and inv mice. *Mol Cell* **4**, 459-468 (1999).

81. Jauregui, A.R. & Barr, M.M. Functional characterization of the C. elegans nephrocystins NPHP-1 and NPHP-4 and their role in cilia and male sensory behaviors. *Exp Cell Res* **305**, 333-342 (2005).

82. Nurnberger, J., Bacallao, R.L. & Phillips, C.L. Inversin forms a complex with catenins and N-cadherin in polarized epithelial cells. *Mol Biol Cell* **13**, 3096-3106 (2002).

83. Morgan, D. et al. Expression analyses and interaction with the anaphase promoting complex protein Apc2 suggest a role for inversin in primary cilia and involvement in the cell cycle. *Hum Mol Genet* **11**, 3345-3350 (2002).

84. Simons, M. et al. Inversin, the gene product mutated in nephronophthisis type II, functions as a molecular switch between Wnt signaling pathways. *Nat Genet* **37**, 537-543 (2005).

85. Otto, E. et al. A gene mutated in nephronophthisis and retinitis pigmentosa encodes a novel protein, nephroretinin, conserved in evolution. *Am J Hum Genet* **71**, 1161-1167 (2002).

86. Matsuzaka, T. et al. Cerebro-oculo-hepato-renal syndrome (Arima' syndrome): a distinct clinicopathological entity. *J Child Neurol* **1**, 338-346 (1986).

87. Kumada, S. et al. Renal disease in Arima syndrome is nephronophthisis as in other Joubert-related Cerebello-oculo-renal syndromes. *Am J Med Genet A* **131**, 71-76 (2004).

88. Beales, P.L., Warner, A.M., Hitman, G.A., Thakker, R. & Flinter, F.A. Bardet-Biedl syndrome: a molecular and phenotypic study of 18 families. *J Med Genet* **34**, 92-98 (1997).

89. Katsanis, N. The oligogenic properties of Bardet-Biedl syndrome. *Hum Mol Genet* **13 Spec No 1**, R65-71 (2004).

90. Beales, P.L. Lifting the lid on Pandora's box: the Bardet-Biedl syndrome. *Curr Opin Genet Dev* **15**, 315-323 (2005).

91. Rizzo, J.F., 3rd, Berson, E.L. & Lessell, S. Retinal and neurologic findings in the Laurence-Moon-Bardet-Biedl phenotype. *Ophthalmology* **93**, 1452-1456 (1986).

92. Hauser, C., Rojas, C., Roth, A., Schmied, E. & Saurat, J.H. A patient with features of both Bardet-Biedl and Alstrom syndromes. *Eur J Pediatr* **149**, 783-785 (1990).

93. Baskin, E. et al. Cerebellar vermis hypoplasia in a patient with Bardet-Biedl syndrome. *J Child Neurol* **17**, 385-387 (2002).

94. Badano, J.L. et al. Identification of a novel Bardet-Biedl syndrome protein, BBS7, that shares structural features with BBS1 and BBS2. *Am J Hum Genet* **72**, 650-658 (2003).

95. Chiang, A.P. et al. Comparative genomic analysis identifies an ADP-ribosylation factor-like gene as the cause of Bardet-Biedl syndrome (BBS3). *Am J Hum Genet* **75**, 475-484 (2004).

96. Katsanis, N. et al. Mutations in MKKS cause obesity, retinal dystrophy and renal malformations associated with Bardet-Biedl syndrome. *Nat Genet* **26**, 67-70 (2000).

97. Mykytyn, K. et al. Identification of the gene that, when mutated, causes the human obesity syndrome BBS4. *Nat Genet* **28**, 188-191 (2001).

98. Mykytyn, K. et al. Identification of the gene (BBS1) most commonly involved in Bardet-Biedl syndrome, a complex human obesity syndrome. *Nat Genet* **31**, 435-438 (2002).

99. Slavotinek, A.M. et al. Mutations in MKKS cause Bardet-Biedl syndrome. *Nat Genet* **26**, 15-16 (2000).

100. Nishimura, D.Y. et al. Positional cloning of a novel gene on chromosome 16q causing Bardet-Biedl syndrome (BBS2). *Hum Mol Genet* **10**, 865-874 (2001).

101. Kulaga, H.M. et al. Loss of BBS proteins causes anosmia in humans and defects in olfactory cilia structure and function in the mouse. *Nat Genet* **36**, 994-998 (2004).

102. Nachury, M.V. et al. A core complex of BBS proteins cooperates with the GTPase Rab8 to promote ciliary membrane biogenesis. *Cell* **129**, 1201-13 (2007).

103. den Hollander, A.I., Roepman, R., Koenekoop, R.K. & Cremers, F.P. Leber congenital amaurosis: genes, proteins and disease mechanisms. *Prog Retin Eye Res* **27**, 391-419 (2008).

104. den Hollander, A.I. et al. Mutations in the CEP290 (NPHP6) gene are a frequent cause of Leber congenital amaurosis. *Am J Hum Genet* **79**, 556-61 (2006).

105. den Hollander, A.I. et al. Mutations in LCA5, encoding the ciliary protein lebercilin, cause Leber congenital amaurosis. *Nat Genet* **39**, 889-95 (2007).

106. Dryja, T.P. et al. Null RPGRIP1 alleles in patients with Leber congenital amaurosis. *Am J Hum Genet* **68**, 1295-8 (2001).

107. Mataftsi, A. et al. Novel TULP1 mutation causing leber congenital amaurosis or early onset retinal degeneration. *Invest Ophthalmol Vis Sci* **48**, 5160-7 (2007).

108. Perrault, I. et al. Spectrum of NPHP6/CEP290 mutations in Leber congenital amaurosis and delineation of the associated phenotype. *Hum Mutat* **28**, 416 (2007).

109. Maria, B.L. et al. Molar tooth sign in Joubert syndrome: clinical, radiologic, and pathologic significance. *J Child Neurol* **14**, 368-376 (1999).

110. Thomas, K.R., Musci, T.S., Neumann, P.E. & Capecchi, M.R. Swaying is a mutant allele of the proto-oncogene Wnt-1. *Cell* **67**, 969-976 (1991).

111. Meyers, E.N., Lewandoski, M. & Martin, G.R. An Fgf8 mutant allelic series generated by Cre- and Flp-mediated recombination. *Nat Genet* **18**, 136-141 (1998).

112. Wurst, W., Auerbach, A.B. & Joyner, A.L. Multiple developmental defects in Engrailed-1 mutant mice: an early mid-hindbrain deletion and patterning defects in forelimbs and sternum. *Development* **120**, 2065-2075 (1994).

113. Joyner, A.L., Herrup, K., Auerbach, B.A., Davis, C.A. & Rossant, J. Subtle cerebellar phenotype in mice homozygous for a targeted deletion of the En-2 homeobox. *Science* **251**, 1239-1243 (1991).

114. Blair, I.P., Gibson, R.R., Bennett, C.L. & Chance, P.F. Search for genes involved in Joubert syndrome: evidence that one or more major loci are yet to be identified and exclusion of candidate genes EN1, EN2, FGF8, and BARHL1. *Am J Med Genet* **107**, 190-196 (2002).

115. Pellegrino, J.E., Lensch, M.W., Muenke, M. & Chance, P.F. Clinical and molecular analysis in Joubert syndrome. *Am J Med Genet* **72**, 59-62 (1997).

116. Aruga, J. The role of Zic genes in neural development. *Mol Cell Neurosci* **26**, 205-221 (2004).

117. Grinberg, I. & Millen, K.J. The ZIC gene family in development and disease. *Clin Genet* **67**, 290-296 (2005).

118. Aruga, J. et al. Mouse Zic1 is involved in cerebellar development. *J Neurosci* **18**, 284-293 (1998).

119. Ogura, H., Aruga, J. & Mikoshiba, K. Behavioral abnormalities of Zic1 and Zic2 mutant mice: implications as models for human neurological disorders. *Behav Genet* **31**, 317-324 (2001).

120. Bennett, C.L. et al. Joubert syndrome: a haplotype segregation strategy and exclusion of the zinc finger protein of cerebellum 1 (ZIC1) gene. *Am J Med Genet A* **125**, 117-124; discussion 117 (2004).

121. Grinberg, I. et al. Heterozygous deletion of the linked genes ZIC1 and ZIC4 is involved in Dandy-Walker malformation. *Nat Genet* **36**, 1053-1055 (2004).

122. Bielas, S.L. et al. Mutations in INPP5E, encoding inositol polyphosphate-5-phosphatase E, link phosphatidyl inositol signaling to the ciliopathies. *Nat Genet* **41**, 1032-6 (2009).

123. Saar, K. et al. Homozygosity mapping in families with Joubert syndrome identifies a locus on chromosome 9q34.3 and evidence for genetic heterogeneity. *Am J Hum Genet* **65**, 1666-1671 (1999).

124. Keeler, L.C. et al. Linkage analysis in families with Joubert syndrome plus oculo-renal involvement identifies the CORS2 locus on chromosome 11p12-q13.3. *Am J Hum Genet* **73**, 656-662 (2003).

125. Dixon-Salazar, T. et al. Mutations in the AHI1 gene, encoding jouberin, cause Joubert syndrome with cortical polymicrogyria. *Am J Hum Genet* **75**, 979-987 (2004).

126. Ferland, R.J. et al. Abnormal cerebellar development and axonal decussation due to mutations in AHI1 in Joubert syndrome. *Nat Genet* **36**, 1008-1013 (2004).

127. Baala, L. et al. The Meckel-Gruber syndrome gene, MKS3, is mutated in Joubert syndrome. *Am J Hum Genet* **80**, 186-94 (2007).

128. Delous, M. et al. The ciliary gene RPGRIP1L is mutated in cerebello-oculo-renal syndrome (Joubert syndrome type B) and Meckel syndrome. *Nat Genet* **39**, 875-81 (2007).

129. Arts, H.H. et al. Mutations in the gene encoding the basal body protein RPGRIP1L, a nephrocystin-4 interactor, cause Joubert syndrome. *Nat Genet* **39**, 882-8 (2007).

130. Cantagrel, V. et al. Mutations in the cilia gene ARL13B lead to the classical form of Joubert syndrome. *Am J Hum Genet* **83**, 170-9 (2008).

131. Gorden, N.T. et al. CC2D2A is mutated in Joubert syndrome and interacts with the ciliopathy-associated basal body protein CEP290. *Am J Hum Genet* **83**, 559-71 (2008).

132. Coene, K.L. et al. OFD1 is mutated in X-linked Joubert syndrome and interacts with LCA5-encoded lebercilin. *Am J Hum Genet* **85**, 465-81 (2009).

133. Poirier, Y., Kozak, C. & Jolicoeur, P. Identification of a common helper provirus integration site in Abelson murine leukemia virus-induced lymphoma DNA. *J Virol* **62**, 3985-3992 (1988).

134. Jiang, X., Hanna, Z., Kaouass, M., Girard, L. & Jolicoeur, P. Ahi-1, a novel gene encoding a modular protein with WD40-repeat and SH3 domains, is targeted by the Ahi-1 and Mis-2 provirus integrations. *J Virol* **76**, 9046-9059 (2002).

135. Smith, T.F., Gaitatzes, C., Saxena, K. & Neer, E.J. The WD repeat: a common architecture for diverse functions. *Trends Biochem Sci* **24**, 181-5 (1999).

136. Mayer, B.J. SH3 domains: complexity in moderation. *J Cell Sci* **114**, 1253-1263 (2001).

137. Jiang, X. et al. Deregulated expression in Ph+ human leukemias of AHI-1, a gene activated by insertional mutagenesis in mouse models of leukemia. *Blood* **103**, 3897-3904 (2004).

138. Ringrose, A. et al. Evidence for an oncogenic role of AHI-1 in Sezary syndrome, a leukemic variant of human cutaneous T-cell lymphomas. *Leukemia* **20**, 1593-601 (2006).

139. Zhou, L.L. et al. AHI-1 interacts with BCR-ABL and modulates BCR-ABL transforming activity and imatinib response of CML stem/progenitor cells. *J Exp Med* **205**, 2657-71 (2008).

140. Alaerts, M. & Del-Favero, J. Searching genetic risk factors for schizophrenia and bipolar disorder: learn from the past and back to the future. *Hum Mutat* **30**, 1139-52 (2009).

141. Amann-Zalcenstein, D. et al. AHI1, a pivotal neurodevelopmental gene, and C6orf217 are associated with susceptibility to schizophrenia. *Eur J Hum Genet* **14**, 1111-9 (2006).

142. Ingason, A. et al. Support for involvement of the AHI1 locus in schizophrenia. *Eur J Hum Genet* **15**, 988-91 (2007).

143. Alvarez Retuerto, A.I. et al. Association of common variants in the Joubert syndrome gene (AHI1) with autism. *Hum Mol Genet* **17**, 3887-96 (2008).

144. Fuchs, J.L. & Schwark, H.D. Neuronal primary cilia: a review. *Cell Biol Int* **28**, 111-118 (2004).

145. Whitfield, J.F. The neuronal primary cilium--an extrasynaptic signaling device. *Cell Signal* **16**, 763-767 (2004).

146. Vigh-Teichmann, I., Vigh, B. & Aros, B. Ciliated perikarya, "peptidergic" synapses and supraependymal structures in the guinea pig hypothalamus. *Acta Biol* **31**, 373-394 (1980).

147. Del Cerro, M.P. & Snider, R.S. The Purkinje cell cilium. *Anat Rec* **165**, 127-130 (1969).

148. Del Cerro, M.P. & Snider, R.S. Studies on the developing cerebellum. II. The ultrastructure of the external granular layer. *J Comp Neurol* **144**, 131-164 (1972).

149. Praetorius, H.A. & Spring, K.R. Bending the MDCK cell primary cilium increases intracellular calcium. *J Membr Biol* **184**, 71-79 (2001).

150. Praetorius, H.A., Frokiaer, J., Nielsen, S. & Spring, K.R. Bending the primary cilium opens Ca2+-sensitive intermediate-conductance K+ channels in MDCK cells. *J Membr Biol* **191**, 193-200 (2003).

151. Handel, M. et al. Selective targeting of somatostatin receptor 3 to neuronal cilia. *Neuroscience* **89**, 909-926 (1999).

152. Schulz, S., Handel, M., Schreff, M., Schmidt, H. & Hollt, V. Localization of five somatostatin receptors in the rat central nervous system using subtype-specific antibodies. *J Physiol Paris* **94**, 259-264 (2000).

153. Brailov, I. et al. Localization of 5-HT(6) receptors at the plasma membrane of neuronal cilia in the rat brain. *Brain Res* **872**, 271-275 (2000).

154. Spassky, N. et al. Primary cilia are required for cerebellar development and Shh-dependent expansion of progenitor pool. *Dev Biol* **317**, 246-59 (2008).

155. Han, Y.G. et al. Hedgehog signaling and primary cilia are required for the formation of adult neural stem cells. *Nat Neurosci* **11**, 277-84 (2008).

156. Chizhikov, V.V. et al. Cilia proteins control cerebellar morphogenesis by promoting expansion of the granule progenitor pool. *J Neurosci* **27**, 9780-9 (2007).

157. Davenport, J.R. et al. Disruption of intraflagellar transport in adult mice leads to obesity and slow-onset cystic kidney disease. *Curr Biol* **17**, 1586-94 (2007).

158. Horst, C.J., Johnson, L.V. & Besharse, J.C. Transmembrane assemblage of the photoreceptor connecting cilium and motile cilium transition zone contain a common immunologic epitope. *Cell Motil Cytoskeleton* **17**, 329-44 (1990).

159. Molday, R.S. Photoreceptor membrane proteins, phototransduction, and retinal degenerative diseases. The Friedenwald Lecture. *Invest Ophthalmol Vis Sci* **39**, 2491-513 (1998).

160. Pepe, I.M. Recent advances in our understanding of rhodopsin and phototransduction. *Prog Retin Eye Res* **20**, 733-59 (2001).

161. Marszalek, J.R. et al. Genetic evidence for selective transport of opsin and arrestin by kinesin-II in mammalian photoreceptors. *Cell* **102**, 175-87 (2000).

162. Pazour, G.J. et al. The intraflagellar transport protein, IFT88, is essential for vertebrate photoreceptor assembly and maintenance. *J Cell Biol* **157**, 103-13 (2002).

163. Sukumaran, S. & Perkins, B.D. Early defects in photoreceptor outer segment morphogenesis in zebrafish ift57, ift88 and ift172 Intraflagellar Transport mutants. *Vision Res* **49**, 479-89 (2009).

164. Tsujikawa, M. & Malicki, J. Intraflagellar transport genes are essential for differentiation and survival of vertebrate sensory neurons. *Neuron* **42**, 703-16 (2004).

165. Bhowmick, R. et al. Photoreceptor IFT Complexes Containing Chaperones, Guanylyl Cyclase 1 and Rhodopsin. *Traffic* (2009).

166. Yoshimura, S., Egerer, J., Fuchs, E., Haas, A.K. & Barr, F.A. Functional dissection of Rab GTPases involved in primary cilium formation. *J Cell Biol* **178**, 363-9 (2007).

167. Deretic, D. et al. rab8 in retinal photoreceptors may participate in rhodopsin transport and in rod outer segment disk morphogenesis. *J Cell Sci* **108 (Pt 1)**, 215-24 (1995).

168. Moritz, O.L. et al. Mutant rab8 Impairs docking and fusion of rhodopsin-bearing post-Golgi membranes and causes cell death of transgenic Xenopus rods. *Mol Biol Cell* **12**, 2341-51 (2001).

169. Chuang, J.Z., Zhao, Y. & Sung, C.H. SARA-regulated vesicular targeting underlies formation of the light-sensing organelle in mammalian rods. *Cell* **130**, 535-47 (2007).

170. Steinberg, R.H., Fisher, S.K. & Anderson, D.H. Disc morphogenesis in vertebrate photoreceptors. *J Comp Neurol* **190**, 501-8 (1980).

171. Altschul, S.F., Gish, W., Miller, W., Myers, E.W. & Lipman, D.J. Basic local alignment search tool. *J Mol Biol* **215**, 403-10 (1990).

172. Fujita, S. Quantitative analysis of cell proliferation and differentiation in the cortex of the postnatal mouse cerebellum. *J Cell Biol* **32**, 277-87 (1967).

173. Blacque, O.E. et al. Loss of C. elegans BBS-7 and BBS-8 protein function results in cilia defects and compromised intraflagellar transport. *Genes Dev* **18**, 1630-1642 (2004).

174. Bishop, G.A., Berbari, N.F., Lewis, J. & Mykytyn, K. Type III adenylyl cyclase localizes to primary cilia throughout the adult mouse brain. *J Comp Neurol* **505**, 562-71 (2007).

175. Caspary, T., Larkins, C.E. & Anderson, K.V. The graded response to Sonic Hedgehog depends on cilia architecture. *Dev Cell* **12**, 767-78 (2007).

176. Koizumi, H., Tanaka, T. & Gleeson, J.G. Doublecortin-like kinase functions with doublecortin to mediate fiber tract decussation and neuronal migration. *Neuron* **49**, 55-66 (2006).

177. Lakso, M. et al. Efficient in vivo manipulation of mouse genomic sequences at the zygote stage. *Proc Natl Acad Sci U S A* **93**, 5860-5 (1996).

178. Hatten, M.E. Neuronal regulation of astroglial morphology and proliferation in vitro. *J Cell Biol* **100**, 384-96 (1985).

179. Higginbotham, H., Bielas, S., Tanaka, T. & Gleeson, J.G. Transgenic mouse line with green-fluorescent protein-labeled Centrin 2 allows visualization of the centrosome in living cells. *Transgenic Res* **13**, 155-64 (2004).

180. Wolfrum, U. & Salisbury, J.L. Expression of centrin isoforms in the mammalian retina. *Exp Cell Res* **242**, 10-7 (1998).

181. Fliegauf, M. et al. Nephrocystin specifically localizes to the transition zone of renal and respiratory cilia and photoreceptor connecting cilia. *J Am Soc Nephrol* **17**, 2424-33 (2006).

182. Humphries, M.M. et al. Retinopathy induced in mice by targeted disruption of the rhodopsin gene. *Nat Genet* **15**, 216-9 (1997).

183. Lem, J. et al. Morphological, physiological, and biochemical changes in rhodopsin knockout mice. *Proc Natl Acad Sci U S A* **96**, 736-41 (1999).

184. Gross, A.K. et al. Defective development of photoreceptor membranes in a mouse model of recessive retinal degeneration. *Vision Res* **46**, 4510-8 (2006).

185. Burns, M.E. & Arshavsky, V.Y. Beyond counting photons: trials and trends in vertebrate visual transduction. *Neuron* **48**, 387-401 (2005).

186. Deretic, D. A role for rhodopsin in a signal transduction cascade that regulates membrane trafficking and photoreceptor polarity. *Vision Res* **46**, 4427-33 (2006).

187. Matsuda, T. & Cepko, C.L. Electroporation and RNA interference in the rodent retina in vivo and in vitro. *Proc Natl Acad Sci U S A* **101**, 16-22 (2004).

188. Matsuda, T. & Cepko, C.L. Controlled expression of transgenes introduced by in vivo electroporation. *Proc Natl Acad Sci U S A* **104**, 1027-32 (2007).

189. Liang, Y. et al. Rhodopsin signaling and organization in heterozygote rhodopsin knockout mice. *J Biol Chem* **279**, 48189-96 (2004).

190. Tronche, F. et al. Disruption of the glucocorticoid receptor gene in the nervous system results in reduced anxiety. *Nat Genet* **23**, 99-103 (1999).

191. Marquardt, T. et al. Pax6 is required for the multipotent state of retinal progenitor cells. *Cell* **105**, 43-55 (2001).

192. El Bradey, M. et al. Preventive versus treatment effect of AG3340, a potent matrix metalloproteinase inhibitor in a rat model of choroidal neovascularization. *J Ocul Pharmacol Ther* **20**, 217-36 (2004).

193. Lancaster, M.A. et al. Impaired Wnt-beta-catenin signaling disrupts adult renal homeostasis and leads to cystic kidney ciliopathy. *Nat Med* (2009).

194. Hong, D.H. et al. RPGR isoforms in photoreceptor connecting cilia and the transitional zone of motile cilia. *Invest Ophthalmol Vis Sci* **44**, 2413-21 (2003).

195. Liu, Q. et al. Identification and subcellular localization of the RP1 protein in human and mouse photoreceptors. *Invest Ophthalmol Vis Sci* **43**, 22-32 (2002).

196. Eley, L. et al. Jouberin localizes to collecting ducts and interacts with nephrocystin-1. *Kidney Int* **74**, 1139-49 (2008).

197. Konrad, M. et al. Large homozygous deletions of the 2q13 region are a major cause of juvenile nephronophthisis. *Hum Mol Genet* **5**, 367-71 (1996).

198. Jiang, S.T. et al. Essential role of nephrocystin in photoreceptor intraflagellar transport in mouse. *Hum Mol Genet* **18**, 1566-77 (2009).

199. Sunyaev, S. et al. Prediction of deleterious human alleles. *Hum Mol Genet* **10**, 591-7 (2001).

200. Yue, P., Melamud, E. & Moult, J. SNPs3D: candidate gene and SNP selection for association studies. *BMC Bioinformatics* **7**, 166 (2006).

201. Sung, C.H., Schneider, B.G., Agarwal, N., Papermaster, D.S. & Nathans, J. Functional heterogeneity of mutant rhodopsins responsible for autosomal dominant retinitis pigmentosa. *Proc Natl Acad Sci U S A* **88**, 8840-4 (1991).

202. Tory, K. et al. High NPHP1 and NPHP6 mutation rate in patients with Joubert syndrome and nephronophthisis: potential epistatic effect of NPHP6 and AHI1 mutations in patients with NPHP1 mutations. *J Am Soc Nephrol* **18**, 1566-75 (2007).

203. Kroes, H.Y. et al. DNA analysis of AHI1, NPHP1 and CYCLIN D1 in Joubert syndrome patients from the Netherlands. *Eur J Med Genet* **51**, 24-34 (2008).

204. Caridi, G. et al. Renal-retinal syndromes: association of retinal anomalies and recessive nephronophthisis in patients with homozygous deletion of the NPH1 locus. *Am J Kidney Dis* **32**, 1059-62 (1998).

205. Spielman, R.S., McGinnis, R.E. & Ewens, W.J. Transmission test for linkage disequilibrium: the insulin gene region and insulin-dependent diabetes mellitus (IDDM). *Am J Hum Genet* **52**, 506-16 (1993).

206. Hsiao, Y.C. et al. Ahi1, whose human ortholog is mutated in Joubert syndrome, is required for Rab8a localization, ciliogenesis and vesicle trafficking. *Hum Mol Genet* **18**, 3926-41 (2009).

207. Khanna, H. et al. A common allele in RPGRIP1L is a modifier of retinal degeneration in ciliopathies. *Nat Genet* (2009).

208. Hooper, M., Hardy, K., Handyside, A., Hunter, S. & Monk, M. HPRT-deficient (Lesch-Nyhan) mouse embryos derived from germline colonization by cultured cells. *Nature* **326**, 292-5 (1987).

209. Fleiss, J.L., Levin, B.A. & Paik, M.C. *Statistical methods for rates and proportions*, xxvii, 760 (J. Wiley, Hoboken, N.J., 2003).

210. Jin, H. et al. The conserved Bardet-Biedl syndrome proteins assemble a coat that traffics membrane proteins to cilia. *Cell* **141**, 1208-19.